Am J Nucl Med Mol Imaging 2018;8(3):200-227
www.ajnmmi.us /ISSN:2160-8407/ajnmmi0079469

Review Article

Searching for novel PET radiotracers: imaging cardiac perfusion, metabolism and inflammation

Caitlund Q Davidson[1], Christopher P Phenix[2], TC Tai[3], Neelam Khaper[1,4], Simon J Lees[1,4]

[1]Department of Biology, Lakehead University, Thunder Bay, Ontario, Canada; [2]Department of Chemistry, University of Saskatchewan, Saskatoon, Saskatchewan, Canada; [3]Medical Sciences Division, Northern Ontario School of Medicine, Laurentian University, Sudbury, Ontario, Canada; [4]Medical Sciences Division, Northern Ontario School of Medicine, Lakehead University, Thunder Bay, Ontario, Canada

Received April 3, 2018; Accepted May 20, 2018; Epub June 5, 2018; Published June 15, 2018

Abstract: Advances in medical imaging technology have led to an increased demand for radiopharmaceuticals for early and accurate diagnosis of cardiac function and diseased states. Myocardial perfusion, metabolism, and hypoxia positron emission tomography (PET) imaging radiotracers for detection of cardiac disease lack specificity for targeting inflammation that can be an early indicator of cardiac disease. Inflammation can occur at all stages of cardiac disease and currently, ^{18}F-fluorodeoxyglucose (FDG), a glucose analog, is the standard for detecting myocardial inflammation. ^{18}F-FDG has many ideal characteristics of a radiotracer but lacks the ability to differentiate between glucose uptake in normal cardiomyocytes and inflammatory cells. Developing a PET radiotracer that differentiates not only between inflammatory cells and normal cardiomyocytes, but between types of immune cells involved in inflammation would be ideal. This article reviews current PET radiotracers used in cardiac imaging, their limitations, and potential radiotracer candidates for imaging cardiac inflammation in early stages of development of acute and chronic cardiac diseases. The select radiotracers reviewed have been tested in animals and/or show potential to be developed as a radiotracer for the detection of cardiac inflammation by targeting the enzymatic activities or subpopulations of macrophages that are recruited to an injured or infected site.

Keywords: Positron emission tomography (PET), radiotracer candidates, myocardial perfusion, metabolism, cardiac disease, cardiac inflammation, inflammatory cells, animal models, macrophages

Introduction

Positron emission tomography (PET) is a nuclear-based modality used for decades as an important clinical tool to non-invasively image blood flow [1, 2], cardiac tissue metabolism [3, 4] and receptor expression [5, 6]. PET requires the injection of a radioactive tracer, labeled with a short-lived radioisotope, that upon decay emits a positron that annihilates with an electron to release coincident photons that are detected by a PET camera. Although single-photon emission computed tomography (SPECT) is less expensive and more commonly used in nuclear medicine departments, a recent expansion in the use of PET for cardiac imaging has resulted from the increasing availability of new PET cameras, PET radiotracers and cyclotron facilities capable of producing the short-lived isotopes needed for labeling chemistry. PET has proven to be a superior technique for molecular imaging due to its accurate attenuation correction, higher spatial and temporal resolution, higher sensitivity, quantitative abilities coupled with lower radiation risk due to the use of short-lived isotopes like carbon-11 (20 min), fluorine-18 (110 min) and rubidium-82 (76 secs) [7, 8]. Further, PET appears to have improved diagnostic accuracy compared to SPECT lowering the overall costs of therapy and improved outcomes [9, 10].

Advances in medical imaging technology have led to an increased demand for radiopharmaceuticals for early and accurate diagnosis of organ function and diseased states. The use of cyclotron produced PET tracers in clinical cardiac imaging has been historically limited due to the requirement of a local cyclotron and radiopharmacy and the challenges associated

Table 1. Half-lives of some PET radioisotopes useful for cardiac imaging

Radioisotope	Half-life (minutes)
^{18}Fluorine	109.8
^{64}Copper	762
^{11}Carbon	20
^{68}Gallium	68
^{82}Rubidium	1.27
^{15}Oxygen	2.06
^{13}Nitrogen	9.97

with the transportation of radiotracers labeled with short-lived PET isotopes to distant locations. However, the International Atomic Energy Agency published statistics in 2006, documenting 80 cyclotrons present in North America. In the last decade, the number of cyclotrons has doubled improving availability and the ease of production of tracers for PET imaging with an estimated 1200 cyclotron facilities that produce medical imaging isotopes world-wide.

Hybrid systems that combine PET with computed tomography (CT) are now routinely found in most nuclear medicine departments, although systems that have PET combined with magnetic resonance imaging (MRI) are appearing at select research intensive sites. The combination of PET with CT allows for the visualization of biological processes facilitated by PET with simultaneous anatomical imaging to identify and determine localization of the tracer uptake in specific tissues and organs. PET/CT is widely used in clinical oncology but also incorporated into clinical cardiology for the detection of coronary artery disease [11, 12]. While there are benefits, including better image resolution than with PET alone and reduced image acquisition time resulting in high patient throughput, the addition of CT significantly increases the amount of radiation exposure to the patient and in most cases, exceeds the measured dose from the injected PET radiotracer [13]. As a consequence, PET/MRI is becoming increasingly available since anatomic detail and soft tissue contrast anatomical images are produced without the additional radiation dose resulting from PET/CT. It important to acknowledge that PET/MRI cannot be used on patients that have implanted devices [14].

PET radiotracers for cardiac imaging

PET uses radiolabeled probes to measure the expression of molecular markers, metabolic and physiological processes at different stages of disease [15]. Many radiotracers have been developed and evaluated in preclinical imaging experiments but few have made it into routine human application for reasons including the cost of animal and clinical trials, company's unwillingness to purchase diagnostic agents that will be used once or twice, and the tracers may lack one or more characteristics that make an ideal PET imaging probe [15]. A PET radiotracer should have high specificity to a molecular target, for example a specific enzyme, biomarker, or transport protein associated with a particular cell population and should have low non-specific uptake into other tissues. Another ideal characteristic is high metabolic stability to prevent the probe from being degraded by enzymes before imaging can be done. A radiotracer should have high affinity for target tissue to achieve sufficient accumulation of the probe for quantitative imaging and analysis. High and rapid uptake of tracer into target tissues followed by long retention time is ideal for high contrast ratio of target-to-background ensuring appropriate analysis of images. Quality of the images is also dependent on the positron range before annihilation [16]. Shorter positron ranges produce higher resolution images [17]. Low production cost and availability of the probes are also important characteristics of an ideal probe. Finally, safety is a concern and therefore probes should have low toxicity and the shortest feasible half-life to keep radiation exposure to a minimum [18, 19]. **Table 1** shows the half-lives of some radioisotopes useful for cardiac imaging.

In some cases, it is important for imaging to be done under normal resting conditions, as well as, following a stress. Stress tests involve cardiac imaging after the patient has performed physical exercise on a treadmill or supine bicycle [20-23]. When exercise-induced stress isn't feasible because the length of the test exceeds the radiotracer half-life or patients who cannot exercise, pharmacological stress is induced by administering dipyridamole, adenosine, regadenoson or dobutamine when the patient is ready to be imaged [23, 24]. Like

Table 2. Hypoxia radiotracer targets, structures, and limitations

Name	Functional Target	Structure	Limitations
^{18}F-fluoromisonidazole (^{18}F-FMISO)	Thiol containing intracellular macromolecules	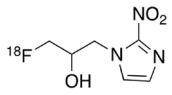	• Slow blood clearance [37] • Long uptake period • Low accumulation in target tissue [34]
Copper(II)-diacetyl-bis(N(4)-methylthiosemicarbazone) (^{64}Cu-ATSM)	Intracellular copper chaperone proteins	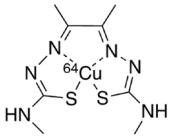	• Useful for detection of extreme hypoxia [60]

exercise, dobutamine increases blood pressure, heart rate and contractility whereas dipyridamole, adenosine, and regadenoson induce coronary vasodilation to increase myocardial blood flow (MBF) [25-28]. Ideally, both stress and rest images can be obtained with one administration of tracer and within the same day.

Fluorine-18 (^{18}F) is generally considered the isotope of choice for radiolabeling potential PET radiotracers. It is produced at every medical cyclotron facility in the world making it widely accessible. In addition, the 109.8-minute half-life of ^{18}F means there is only a few hours to prepare, purify, perform quality control and transport the radiotracer to nearby sites and hospitals that have a PET camera. Another advantage of ^{18}F is that it can be conservatively incorporated into small molecule radiotracers by replacing a hydrogen or hydroxyl group intended to mimic small molecule drugs or natural metabolites without significantly disrupting molecular recognition. In addition, small molecules are typically cleared from tissues, thus sufficient levels of the radiotracer can accumulate into cardiac tissue for quantitative imaging experiments an hour or two after injection without exposing the patient to dangerous levels of radiation.

Similar to ^{18}F, carbon-11 (^{11}C) is an excellent choice for metabolic imaging since it is a small atom and can be incorporated into molecules that are ligands to a protein or metabolized through normal metabolic processes. The large radiometals like copper-64 (^{64}Cu) are typically used for labeling antibodies and proteins that have longer serum half-lives and bind to receptors while generator produced gallium-68 (^{68}Ga) is a convenient isotope for labeling peptides that are quickly cleared from serum. While the very short-lived isotopes like rubidium-82 (^{82}Rb), nitrogen-13 (^{13}N) and oxygen-15 (^{15}O) are useful for perfusion imaging. A long list of radiotracers has been developed for PET imaging of hypoxia, metabolism, inflammation and myocardial perfusion with several others in development in attempt to create suitable PET probes for various physiological and disease processes.

Hypoxia

The heart requires oxygen to produce sufficient ATP to maintain function and viability. Hypoxia, or oxygen deficiency, can lead to metabolic and functional abnormalities in the heart [29]. PET radiotracers that can reveal the presence of hypoxic cells have prognostic and diagnostic value and they measure myocardial viability. Brief ischemic events are reversible but chronic hypoxia can cause the myocardium to become necrotic and non-viable [29]. Therefore, early detection of hypoxia is beneficial. For accurate assessment, it is important that hypoxia tracers are specific to hypoxic cells and are not retained in normal or necrotic cells. Therefore, choosing a target unique to hypoxic cells or utilizing a mechanism specific to hypoxic cells is critical. **Table 2** summarizes the targets, structures and limitations of two common radiotracers used for detecting hypoxia which are discussed in this section.

^{18}F-fluoromisonidazole

^{18}F-fluoromisonidazole (FMISO) is the most commonly used PET tracer for measuring hypoxia in neurology, oncology and cardiology. FMISO enters the cells by passive diffusion across the cell membranes. It accumulates in hypoxic cells with low oxygen levels due to the rapid reduction of the radiotracer from the mitochondrial electron transfer system to generate an electrophilic species that reacts with

cellular proteins and is retained in the local region [30, 31]. Hypoxic cells do not have enough O_2 to oxidize FMISO so the reduced radiotracer remains trapped in the hypoxic cell [32, 33]. Normoxic cells have enough O_2 to oxidize FMISO which allows it to diffuse out of normal cells, thus preventing it from accumulating [33]. Necrotic cells do not have functioning mitochondria for the reduction of the radiotracer and it rapidly diffuses out of the cell. Retention of ^{18}F-FMISO correlates with the severity of hypoxia. This process requires a long uptake period and even then, there is low accumulation of the tracer in target tissue compared to plasma and muscle [34-36].

Tissue oxygenation has been validated in tumors but not in the heart. Use of ^{18}F-FMISO in the heart has been poorly studied and has been limited to animal and *in vitro* studies. It has not gained the same acceptance as a hypoxia tracer in human nuclear cardiac imaging due to the prolonged blood clearance, tissue uptake time and low accumulation levels which make it difficult to decipher normal tissues and blood from the target tissue affecting image quality [32, 37]. Hypoxic cell marker pimonidazole, an immunostain that binds to thiol-containing proteins in hypoxic cells forming intracellular adducts, is used in staining of biopsied tissues and can be a useful validation tool; however, in order to gain information from patients about hypoxia over time, an imaging probe would be useful [38]. Validation of ^{18}F-FMISO accumulating in hypoxic regions have been performed in conjunction with pimonidazole in rabbits with advanced atherosclerosis [39]. Similarly, oncological studies have also used pimonidazole to validate their ^{18}F-FMISO PET imaging results [40]. In comparison to pimonidazole, ^{18}F-FMISO can provide information at a global rather than microscopic level on the distribution of hypoxia [36].

In the heart, ^{18}F-FMISO can detect hypoxic but viable tissue. Its most common use is in characterizing myocardial ischemia and its severity [41, 42]. Tested radiotracers have been able to detect the presence of hypoxia but not differentiate the degree of hypoxia [41, 43]. A canine study examined the ability of ^{18}F-FMISO as a marker of hypoxia and found accumulation in areas of low blood flow like ischemic myocardium but not in necrotic or normally perfused myocardium [41]. The authors further suggest that ^{18}F-FMISO be used for both hypoxia and assessment of oxygen supply for metabolism. The accuracy of ^{18}F-FMISO is dependent on time allowed for bio-distribution, bio-reduction and wash-out [36, 40, 41]. Alternative nitroimidazole tracers to ^{18}F-FMISO have been developed for faster clearance and better tumour-to-background ratio for improved image contrast including ^{18}F-fluoroazomycin arabinoside (^{18}F-FAZA), ^{18}F-2-(2-nitro-1H-imidazol-1-yl)-*N*-(2,2,3,3,3-pentafluoropropyl)-acetamide (^{18}F-EF5),^{18}F-2-(4-((2-nitro-1H-imidazol-1-yl)methyl)-1H-1,2,3-triazol-1-yl)propan-1-ol (^{18}F-HX4), and ^{18}F-fluoroerythronitroimidazole (^{18}F-FETNIM) [44–48]. These tracers have applications mainly for cancer imaging with few studies investigating uptake by hypoxic cells in the heart [44, 49].

^{64}Cu-ATSM

Copper(II)-diacetyl-bis(N(4)-methylthiosemicarbazone) (^{64}Cu-ATSM) is a PET radiotracer used to assess hypoxia in oncology, neurology and cardiology. Bougeois et al. provides an extensive comparison of hypoxia radiopharmaceuticals ^{18}F-FMISO and ^{64}Cu-ATSM that details the labeling process, dosimetry data, mechanisms and image contrast in clinical studies [50]. The use of ^{64}Cu-ATSM for PET imaging in *in vivo* and *in vitro* studies is covered in a report by Vãvere et al. (2007) [51]. ATSM can be labelled with isotopes $^{60/61/62/64}$Cu based on the physical properties required [50, 52]. ^{64}Cu is preferred because it has a sufficient half-life of 12.7 hours and is the most cost effective to produce. Using the cyclotron produced ^{64}Cu, ^{64}Cu-ATSM can be synthesized in a radiopharmacy at high purity and sufficient quantity for clinical purposes [53]. The retention mechanism has been hypothesized by several research groups and is not yet fully known. It is thought that Cu(II)-ATSM diffuses into the cell and is reduced to Cu(I)-ATSM under hypoxic and normoxic conditions [54]. The reduced ^{64}Cu-ATSM is unable to leave the cell and accumulates. However, under normoxic conditions, the reduced complex can be reoxidized and leave the cell.

Two advantages of ^{64}Cu-ATSM are higher cellular uptake and quicker washout from normal tissue, which allows imaging to be done shortly after injection [51, 55]. The low redox potential of ATSM is thought to be responsible for its high

Table 3. Metabolic radiotracers functional targets, structures, and limitations

Name	Functional Target	Structure	Limitations
^{11}C-Acetate	Mono-carboxylate transporter		• Requires on-site or nearby cyclotron • Short half-life
^{11}C-Palmitate	Fatty acid transporter protein	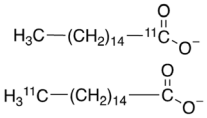	• Requires on-site or nearby cyclotron • Low specificity [4] • Poor image quality [82]
^{18}F-fluorodeoxyglucose (FDG)	Facilitative glucose transporters	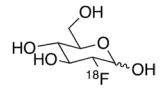	• Low specificity [90]
^{68}Ga-1,4,7,10-tetraazacyclododecane-*N*,*N*',*N*'',*N*'''-tetraacetic acid]-d-Phe1, Tyr3-octreotate (^{68}Ga-DOTATATE)	Somatostatin receptor 2	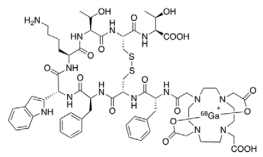	• Uptake limited by SSTR-2 availability [97]

selectivity [56-58]. Selective retention of the tracer requires intact mitochondria and a significantly high concentration of NADH [59]. Therefore, this tracer is only useful for detection of extreme hypoxia [60]. Researchers have also found that derivatives of ATSM with reduced lipophilicity can increase selectivity to better hypoxic-to-normoxic cell contrast [32].

Metabolism and inflammation

Cardiomyocytes can utilize a number of substrates for energy including glucose, fatty acids, lactate, and ketone bodies to maintain cardiac health under changing environmental conditions. Abnormalities in myocardial metabolism is indicative of pathogenesis of heart disease. For example, glucose metabolism in the heart increases under hypoxic conditions [61, 62]. Chronic metabolic adaptations can cause alterations in gene expression, which can lead to the upregulation of proteins and enzymes in metabolic pathways [4]. **Table 3** summarizes the functional targets, structures and limitations of select current metabolic PET radiotracers.

Inflammation plays a role in heart disease and can be an important imaging target to detect and assess severity of heart disease. Inflammation can be present at all stages of development of cardiovascular disease [63]. Infiltrating immune cells, like macrophages, have higher glucose uptake than normal cells and are found at sites of inflammation [64-66]. Developing a PET radiotracer to detect small amounts of inflammation would be beneficial for early detection.

PET imaging can also detect myocardial viability by examining metabolism and myocardial perfusion imaging (discussed below) in combination. Myocardial tissue can be viable but demonstrate decreased perfusion and this may suggest underlying coronary artery disease (CAD). Assessment of myocardial viability can detect areas where revascularization is possible which improves patient prognosis. If a patient has decreased perfusion but viable myocardium, measured separately using a myocardial perfusion imaging radiotracer like ^{82}Rb (discussed later) for perfusion and ^{18}F-fluorodeoxyglucose to measure viability, they are likely to benefit from revascularization whereas patients with nonviable myocardium will not.

^{11}C-acetate

^{11}C-acetate is a versatile radiotracer since it is rapidly taken up into the cell and converted to acetyl-CoA. From there, it has multiple potential pathways including conversion to amino acids, synthesis of fatty acids or oxidation to CO_2 and H_2O. In the myocardium, it enters the tricarboxylic acid cycle and is oxidized to CO_2 for energy production [67]. PET scans are done immediately after injection because of the tracer's short half-life of approximately 20 minutes [68]. For the same reason, use of ^{11}C-acetate is limited due to the need for an on-site or nearby cyclotron. Uptake of ^{11}C-acetate into cardiomyocytes is dependent on MBF but clearance of the tracer quantifies myocardial oxidative metabolism [69-71]. This means that high accumulation of the radiotracer in the myocardium indicates low oxidative metabolism, however low accumulation indicates higher oxidative metabolism because the ^{11}C is rapidly released as $^{11}CO_2$.^{11}C-acetate is the preferred radiotracer for measuring myocardial oxygen consumption with PET.

A review by Grassi et al., thoroughly describes the use of ^{11}C-acetate in oncological imaging [72]. In cardiology, ^{11}C-acetate is used to measure oxidative metabolism and myocardial blood flow [73, 74]. Timmer et al., validated the use of ^{11}C-acetate to measure MBF by comparing MBF values to those from ^{15}O-water studies. They tested four methods and determined that ^{11}C-acetate with a single tissue compartment kinetic model and standardized corrections provided the best results for MBF [75]. Other studies using ^{11}C-acetate have shown promising results in evaluating MBF, oxidative metabolic rate, cardiac output and efficiency under stress/rest conditions [72, 76].

^{11}C-palmitate

^{11}C-palmitate is a labelled free fatty acid used to measure fatty acid metabolism. In nuclear cardiac imaging, it has been used to measure myocardial triglyceride degradation and oxidation [77, 78]. After injection, it binds to serum albumin and is taken up into the myocardium where uptake is dependent on MBF [79]. Slow washout of tracer is indicative of incorporation

into the triglyceride pool whereas rapid washout of tracer is associated with oxidative metabolism of fatty acids [80]. Fatty acid catabolism can be directly assessed by the washout kinetics of ^{11}C-palmitate [80]. The accuracy of measuring fatty acid metabolism is reduced because of back-diffusion out of the cell immediately after uptake [81]. Further disadvantages include lack of specificity, the need for an on-site cyclotron for production, and the poor quality of PET images from spillover that require correction [4, 82]. The spillover effect is when cross-contamination of radioactivity occurs between different regions because of photon scatter during imaging that result in a false result during image analysis [83]. Similar to ^{11}C-acetate, the short half-life of ^{11}C means that the use of ^{11}C-palmitate is typically restricted to locations with or near a cyclotron facility.

^{18}F-FDG

^{18}F-fluorodeoxyglucose (^{18}F-FDG) has been used as an important research radiotracer in the context of oncological, neurological and cardiologic pathologies. ^{18}F-FDG PET has been used for tracking glucose metabolism to test myocardial viability, and imaging myocardial inflammation. ^{18}F-FDG PET can also monitor progression of disease by assessment of perfusion patterns [84]. FDG is a glucose analog that enters cardiomyocytes via glucose transporters, commonly GLUT1 and GLUT4 [85]. Once inside the cell, hexokinase phosphorylates FDG to FDG-6-phosphate. The phosphorylated metabolite is no longer a substrate for GLUT1 and 4, and cannot be further metabolized and therefore accumulates within the cell. Only tissues with high levels of glucose-6-phosphatase can rapidly dephosphorylate FDG-6-phosphate back to FDG, which then can exit the cell and prevent radiotracer accumulation (e.g., liver) [86, 87]. Uptake of ^{18}F-FDG can be influenced by insulin and is therefore dependent on factors related to fed versus fasted state [88, 89].

One advantage of ^{18}F-FDG is its longer half-life compared to ^{11}C labeled radiotracers, which allows transport time from the production site to the imaging site. In addition, active transport and metabolic trapping of ^{18}F-FDG in cells means PET imaging studies can be carried out many hours after production. The ideal time between injection of ^{18}F-FDG and imaging is 45-60 minutes to allow for tissue distribution. Unfortunately, because normal cardiomyocytes also use glucose, ^{18}F-FDG has a low specificity for normal cardiomyocytes and can lead to false positives of glucose uptake and perfusion patterns when assessing disease caused by increased FDG uptake by non-specific infectious or inflammatory processes [90, 91]. Further development of ^{18}F probes for not only glucose metabolism but for the detection of inflammation are needed.

Somatostatin receptors

Somatostatin receptor (SSTR) PET probes are an alternative to ^{18}F-FDG for targeting inflammation. SSTR PET probes have been developed for oncological imaging but have potential purpose in imaging cardiac inflammation. Somatostatin binding to the receptors exert an immunosuppressive effect that may also help in the development of therapeutic strategies [92]. There are 5 SSTR subtypes. SSTR type 2 (SSTR-2) is over-expressed on the surface of activated macrophages providing a potential target for imaging that is more specific for measuring inflammation caused by macrophage infiltration [93, 94]. This type of probe is also capable of detecting proliferating endothelium and angiogenesis [95, 96]. ^{68}Ga-1,4,7,10-tetraazacyclododecane-*N*,*N*',*N*'',*N*'''-tetraacetic acid]-d-Phe1, Tyr3-octreotate (^{68}Ga-DOTATATE) targets subtype 2 and has been used for investigating the distribution of SSTR-2 and tracking inflammation in the development of atherosclerotic plaque [5, 97].

^{68}Ga-DOTATATE binds with high affinity to SSTR-2 [98, 99]. However, uptake is limited by the number of occupied SSTR-2 [97]. This tracer has fast blood clearance and has been found to be superior to ^{18}F-FDG in identifying atherosclerotic high-risk versus low-risk lesions and shows greater specificity as an inflammation imaging target [6]. Repeated imaging is possible within the 68-minute half-life of the tracer [100]. The higher energy of the emitted positron from ^{68}Ga is expected to result in lower image resolution however images are comparable to ^{18}F and have sufficiently high resolution [100, 101]. A significant benefit of using ^{68}Ga-DOTA-peptides for PET imaging is that a daily supply of the isotope for radiolabeling is available from the ^{68}Ge/^{68}Ga generator that is commercially available and can be shipped to a radiopharmacy thus eliminating the need for an

Table 4. Myocardial perfusion tracer targets, structures, and limitations

Name	Functional Target	Structure	Limitations
^{82}Rubidium chloride (^{82}Rb)	Sodium-potassium ATPase	^{82}RbCl	• Low image resolution [103] • Exhibits roll-off phenomenon [116, 117] • Lower myocardial extraction fraction than other perfusion tracers [103, 118, 119]
^{15}O-Water	Circulation between intercellular space and intracellular compartment		• Short half-life • Requires on-site cyclotron • Low resolution [127] • Susceptible to spillover effect [121]
^{13}N-Ammonia	Circulation between intercellular space and intracellular compartment		• Requires on-site or nearby cyclotron • Not practical for stress testing [136]
^{18}F-Flurpiridaz	Mitochondrial complex-1 of the electron transport chain	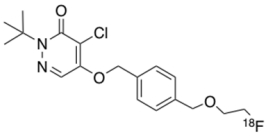	• In Phase 3 of clinical testing • Current research aimed at improving metabolic stability [147]

onsite cyclotron [102]. The generator can last up to one year before replacement is required [102]. Banerjee et al., has reviewed several other radiotracers targeting SSTR's but are not as well studied as ^{68}Ga-DOTATATE for the purpose of identifying cardiac inflammation [100].

Myocardial perfusion imaging

Myocardial perfusion imaging (MPI) tracers are the gold standard for measuring blood flow in the heart with PET. There are several criteria that a tracer must meet to achieve high quality imaging for perfusion analysis. This includes having a high extraction fraction and myocyte retention, unit dose availability from a regional cyclotron, radiotracers labeled with isotopes that have low positron range and high image resolution, possibility of both rest and exercise imaging and absolute quantification of myocardial blood flow [103-105]. Two sets of images are acquired for MPI, one set during rest and one following a stress test. Spillover in the images from the left ventricular blood pool into the myocardium due to the pool spatial resolution of PET is a common problem that requires correction [106]. To correct this problem and improve accuracy of activity measurements, several models of blood poor calculations were introduced [83, 107].

^{82}Rubidium, ^{14}N-ammonia and ^{15}O-water are well established MPI radiotracers for quantitative measurement of MBF that have appropriate dosimetry and safety profiles [18, 108]. The ^{18}F labelled tracer, flurpiridaz, is in late stages of FDA approval and has potential for being an ideal PET MPI radiotracer. The functional targets, structures and limitations of these radiotracers are shown in **Table 4**. The use of PET imaging over other imaging modalities for MPI would likely increase with the development of improved PET radiotracers which minimize short-comings.

^{82}Rubidium

^{82}Rubidium (^{82}Rb), a short-lived isotope with a half-life of 76 seconds, is the most widely used radiopharmaceutical in clinical practice for MPI with PET. Rb is an alkali metal that has similar physical and chemical properties to potassium and can therefore be used to image potassium transport *in vivo* [109-111]. A commercially available strontium-82 (^{82}Sr/^{82}Rb) generator can be used to produce ^{82}Rb allowing PET MPI studies to be performed at locations without nearby access to a cyclotron facility [112]. Shelf-life of the generator is 4 to 5 weeks after which a replacement generator is necessary [112]. After administration by intravenous injection, ^{82}Rb crosses the capillary membrane and is taken up from plasma by myocardial cells through active transport [110]. The short half-life of this tracer usually requires that pharmacological protocols are used instead of the exercise for stress testing [113-115].

^{82}Rb has certain limitations that prevent it from being ideal including having the lowest image resolution of the MPI tracers because of its high positron range (8.6 mm) [103]. Myocardial extraction of ^{82}Rb begins to level off at high blood flow levels and the tracer is no longer able to track blood flow [111, 116]. This is called the roll-off phenomenon [116,

117]. The myocardial extraction fraction of ^{82}Rb is lower than the other PET perfusion tracers at only 65% resulting in a low signal-to-noise ratio between the heart and other tissues [103, 118, 119].

^{15}O-water

^{15}O-water was one of the first radiotracers developed for MPI. It displays almost perfect first-pass extraction fraction resulting in a linear relationship between tracer uptake and flow at high blood flow rates [120-122]. ^{15}O-water is freely diffusible across cell membranes and capillaries, which allows for high uptake but prevents tracer from being retained in the myocardium [120, 123]. For the same reason, it is difficult to decipher between tracer activity in the blood and myocardial tracer uptake since the tracer can easily diffuse into both regions. ^{15}O-water is susceptible to a spill-over effect between the left ventricle blood pool and the myocardial wall because of the limited spatial resolution of PET imaging [121]. Tracer from the blood pool spills into the myocardial regions of interest, falsely elevating tissue tracer concentration. Calculations to correct this problem involve the use of an oxygen-15-labeled carbon monoxide scan, prior to administering ^{15}O-water, to label red blood cells that are confined to the vascular space [121, 124-126]. This scan is subtracted from the ^{15}O-water images giving measures for MBF free from intervascular activity. An additional limitation is the need for an on-site cyclotron because of its short half-life of approximately 2 minutes. With ^{15}O-water, images have low resolution because of low myocardium-to-background contrast ratios from tracer freely diffusing between the myocardium and blood pool [127, 128]. Another downfall due to half-life is the inability to acquire images with physical stress tests because there is not enough time to inject the tracer, exercise and image [129, 130]. Regardless of its strengths, ^{15}O-water has not been FDA approved for MPI with PET.

^{13}N-ammonia

^{13}N-ammonia is another well-known PET radiotracer for measuring MPI. Delivery of this tracer from a cyclotron facility to a PET imaging facility is possible because of the ^{13}N radiolabel half-life of 9.97 minutes; although not ideal. ^{13}N-ammonia has a high first pass myocardial extraction of about 80% and is rapidly cleared from the blood [131]. Ammonia (NH_3) can quickly diffuse across membranes or be actively transported by the sodium-potassium pump [131, 132]. In the myocyte, NH_3 has two potential fates: it can back diffuse into the vascular space and blood or it can be trapped in the myocardium when NH_3 converts to glutamine. Ideal linear uptake of tracer is noted at low level of blood flow but at higher blood flow this tracer experiences the roll-off phenomenon like ^{82}Rb [133, 134]. A shorter positron range (2.5 mm) of ^{13}N enables good quality imaging but physical stress tests are not practical for routine use because of the time interval between tracer injection and start of imaging as well as the acquisition time [21, 135, 136]. In comparison to the previously discussed MPI tracers, ^{13}N presents numerous characteristics of an ideal radiotracer including its high extraction fraction, relatively long half-life and low background activity [126, 131, 137].

^{18}F-flurpiridaz

Over the past several years, ^{18}F labelled analogs have been developed to take advantage of the prolonged half-life and improved image resolution for MPI. ^{18}F-flurpiridaz, previously called ^{18}F-BMS-747158-02, is a structural analog of the insecticide pyridaben that was developed to overcome the need for on-site production and cost of generators as with other MPI radiotracers [138]. It is the only ^{18}F-labeled MPI tracer that is currently in Phase 3 of clinical testing and awaiting FDA approval [138, 139].

^{18}F-flurpiridaz targets mitochondria and therefore, accumulates in mitochondria-rich tissues like the myocardium. The tracer accumulates in metabolically active cardiomyocytes by inhibiting the mitochondrial complex-1 (MC-1). MC-1, located in the inner mitochondrial membrane, is part of the electron transport chain responsible for the coupling of NADH oxidation and the reduction of ubiquinone, to the generation of a proton gradient which is then used for ATP synthesis. ^{18}F-flurpiridaz binds specifically to the PSST subunit of MC-1, the same binding site as ubiquinone [140]. ^{18}F-flurpiridaz binds reversibly to the site and does not affect the viability of the cell by binding. No toxic side effects result from ^{18}F-flurpiridaz since the overall activity of MC-1 is not inhibited due to the

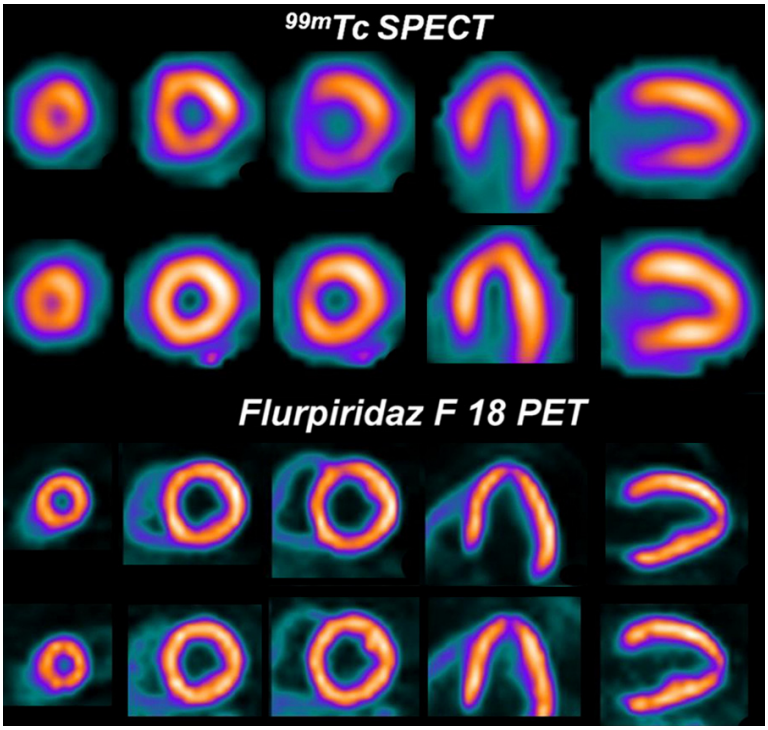

Figure 1. ^{99m}Tc SPECT images (upper rows) and ^{18}F-flurpiridaz PET images (lower rows) from a patient with normal coronary arteries. A false positive reversible inferior defect is present on the ^{99m}Tc SPECT images due to shifting soft-tissue attenuation. The ^{18}F-flurpiridaz PET study, however, provided superior image quality and was normal.

microdoses used for PET imaging. ^{18}F-flurpiridaz exhibits a rapid uptake in active cardiomyocytes and slow washout [138, 140, 141]. It shows excellent potential for being an accurate myocardial perfusion probe based on its almost linear relationship between MBF and radiotracer uptake [138, 141, 142].

^{18}F-flurpiridaz produces higher resolution myocardial perfusion images than SPECT tracers or ^{82}Rb resulting in higher diagnostic confidence in interpretation of the images as shown in **Figure 1** [143]. The images produced are excellent due to the short positron range and higher specificity and sensitivity to detect known or suspected CAD compared to SPECT imaging [140, 143]. ^{18}F-flurpiridaz has several advantages over the other PET MPI tracers including the longer physical half-life of ^{18}F which allows for administration of the radiotracer at the peak of treadmill exercise followed by imaging. Both rest and stress imaging with this tracer can be done within 20-30 minutes whereas with other tracers this is not possible [144-146]. Another advantage is its ability to detect more subtle perfusion defects while having better image contrast due to high uptake in the target tissue (heart) and lower uptake in other tissues like the liver and lungs compared to ^{13}N-ammonia [142, 143, 145]. This is not only beneficial for producing excellent images, but additionally, the radioactive dose to other tissues is not an issue. Although, the heart-to-background contrast is better than ^{13}N-ammonia, there is still room for improvement. Other ^{18}F-labelled pyridaben analogues are being examined to improve metabolic stability and improve liver clearance [147, 148].

PET imaging of cardiovascular disease

Early detection of both acute and chronic cardiac disease is crucial. Most patients remain undiagnosed as they appear asymptomatic. It is thought to be unnecessary to image asymptomatic patients, which leaves cardiovascular diseases to remain undetected and progress from subclinical to symptomatic disease state. Several metabolic and functional changes occur before structural ones are noticed. However, it would be beneficial to detect subclinical changes prior to development of symptoms for a better prognosis. The following section details a few acute and chronic diseases where PET imaging has been found to be useful for early detection of disease.

Acute disease

Myocarditis

Myocarditis is inflammation of the myocardium caused by viral infections, toxins, drugs, or an activated immune system that attacks host antigens that can affect cardiac muscle function and the cardiac conduction system. There is a wide range of clinical presentations and symptoms that can lead to misdiagnosis [149]. Most patients are asymptomatic and do not seek medical assistance [150]. Myocarditis can progress from acute inflammation to chron-

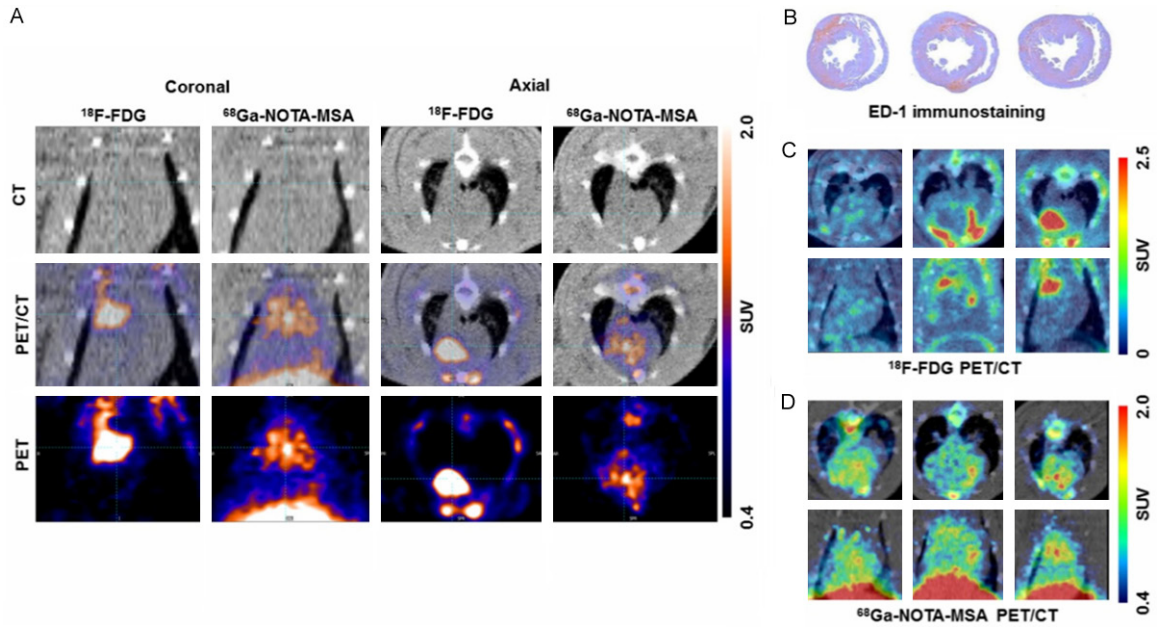

Figure 2. Comparison of ^{18}F-FDG and ^{68}Ga-NOTA-MSA PET for detection of myocardial inflammation in myocarditis. A. The hotspots of myocardial inflammation colocalizes between the ^{18}F-FDG and ^{68}Ga-NOTA-MSA PET scans in some animals. B-D. Different degree of ^{18}F-FDG and ^{68}Ga-NOTA-MSA in spite of the similar degree of inflammatory cell infiltration. B. Similar degree of inflammatory cell infiltration on ED-1 immunostaining. C. Different degree of ^{18}F-FDG uptake between the animals, despite similar degree of inflammatory cell infiltration. D. Similar degree of ^{68}Ga-NOTA-MSA uptake between the animals. SUV, standardized uptake value.

ic inflammation if the pathogen is not eliminated [150]. If acute myocarditis continues to evolve undetected, it can lead to sudden death, heart failure, or dilated cardiomyopathy [149].

Early metabolic changes associated with myocarditis can be detected with PET. As mentioned earlier, PET scanners frequently come as a hybrid system with CT. Combing PET with CT allows imaging of biological processes with anatomic detail [151]. A study that used ^{18}F-FDG and PET/CT found higher specificity and sensitivity when used within 14 days of onset of suspected acute myocarditis compared to 15-60 days after onset [152]. ^{18}F-FDG focal and diffuse patterns of uptake in the left ventricular posterior wall were indicative of inflammation and correlated with results from endomyocardial biopsy, the gold standard method for detection of inflammation [153-155]. This study was limited by its small sample size and therefore could not conclude the use of ^{18}F-FDG PET alone for diagnosis. ^{18}F-FDG can detect active macrophage and lymphocyte activity indicative of inflammation but its ability to detect myocarditis is not clear. Accuracy of inflammation detection can be improved by combining ^{18}F-FDG PET sensitivity with the high spatial resolution of MRI using a PET/MRI system [155]. However with this, comes the limitations mentioned previously.

^{68}Ga-2-(p-isothiocyanatobenzyl)-1, 4,7-triazacyclononane-1, 4,7-triacetic acid mannosylated human serum albumin (NOTA-MSA) was initially developed as a lymph node PET imaging agent but has potential use for detection of acute myocarditis [156]. Lee et al., used this probe for the detection of myocardial inflammation in a rat model of myocarditis as shown in **Figure 2** [157]. This probe targets the mannose receptors on activated infiltrating macrophages. Higher uptake was found in organs with macrophage accumulation including the liver, spleen, bone marrow and myocardium. ^{68}Ga-NOTA-MSA uptake in the left ventricle (LV) was upregulated in myocarditis compared with normal rats. They noted that ^{68}Ga-NOTA-MSA uptake was significantly enhanced earlier in the development of myocarditis before inflammation could be seen on an echocardiograph. The authors suggest ^{68}Ga-NOTA-MSA PET has a potential use for visualizing infiltrating mannose-receptor positive macrophages and early

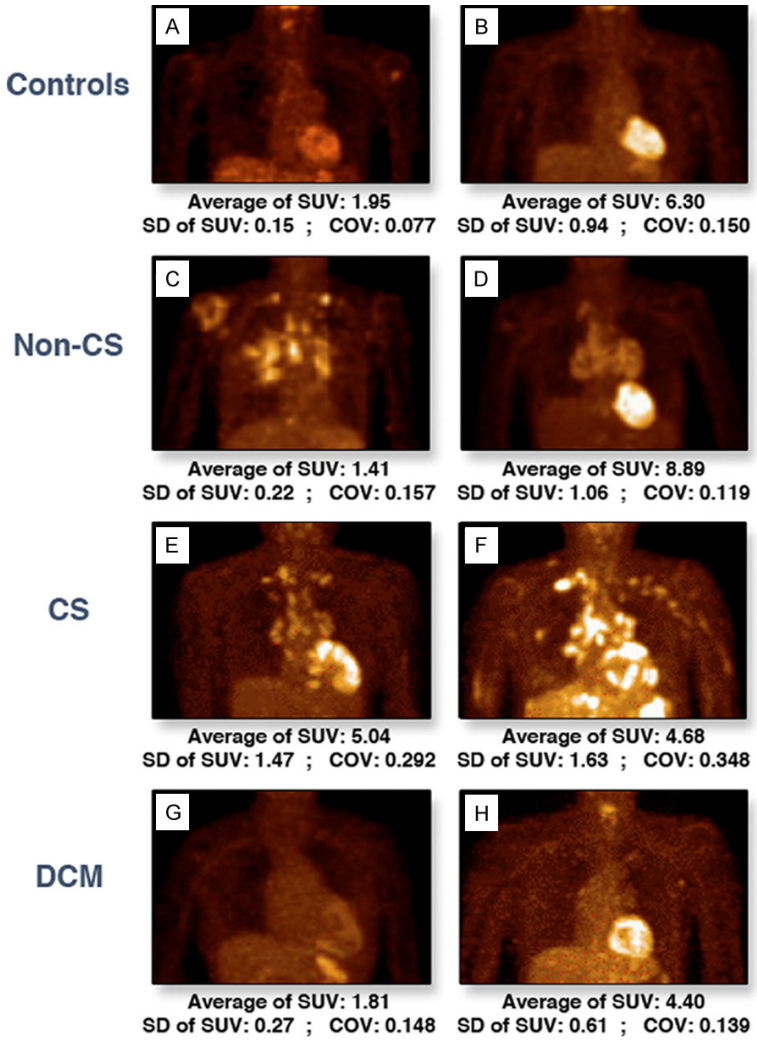

Figure 3. Representative ^{18}F-FDG PET anterior views. The myocardial uptake of ^{18}F-FDG in healthy control subjects (A, B), noncardiac sarcoidosis (C, D), cardiac sarcoidosis (E, F), and dilated cardiomyopathy (G, H) patients. COV = coefficient of variation; CS = cardiac sarcoidosis; DCM = dilated cardiomyopathy; SUV = standardized uptake value.

diagnosis of myocarditis. From this study, it is unknown if this tracer specifically targets myocarditis or whether it targets other disease caused by macrophage infiltration like atherosclerosis [157]. It is also unclear if ^{68}Ga-NOTA-MSA binds to mannose receptors on the macrophages only.

Cardiac sarcoidosis

Cardiac sarcoidosis (CS) is a rare and potentially fatal disease that results from the accumulation of non-caseating granulomas which are a collection of macrophages, lymphocytes and epithelioid cells. The granulomas form around a pathogen or environmental agent to protect the tissue from damage. Sarcoid granulomas can form in the heart and affect the epicardium or pericardium but is most commonly seen in the myocardium. The etiology of CS is still unknown. CS is difficult to detect and underdiagnosed as patients can be asymptomatic [158]. When detected, this disease is associated with poor prognosis but early diagnosis and treatment could improve prognosis.

Known and suspected cases of sarcoidosis are tested for inflammation with ^{18}F-FDG. ^{18}F-FDG PET emerged as a superior technique to ^{67}Ga scintigraphy with higher sensitivity and accuracy for the detection of CS [159-161]. FDG accumulates in sarcoid lesions at sites of macrophage-mediated inflammation where the macrophages are using glucose for energy [90]. Focal or heterogeneous tracer uptake is suggestive of active CS as shown in **Figure 3** [162]. Imaging with ^{18}F-FDG has led to many false positives because of the difficulty in deciphering between normal myocyte uptake and inflammatory cell uptake. Patient protocols including prolonged fasting, dietary restrictions and administration of heparin have been put into place in attempt to reduce false positives by suppressing physiological FDG uptake [163, 164]. Myocardial ^{18}F-FDG uptake caused by inflammation may not be specific to CS and considered indirect evidence of the presence of CS. Therefore, metabolic PET imaging with FDG is compared to perfusion results.

Perfusion deficits in the myocardium can be detected with ^{13}N-ammonia or ^{82}Rb PET. Comparison of myocardial perfusion images with ^{18}F-FDG PET images allows for differentiation between normal myocardium and scarred myocardium, which can rule out coronary heart dis-

ease [165]. Findings can indicate stage of disease progression and if therapy will be useful. Perfusion imaging of tissue viability will detect any damaged tissue by measuring regional MBF at rest and under pharmacological stress.

After detection of CS, steroid therapy is administered but it is only efficient if administered before the development of left ventricular systolic dysfunction and fibrosis [166, 167]. Progression of steroid therapy is tracked using ^{18}F-FDG PET [161]. Lower uptake of the tracer is seen when therapy is working to resolve inflammation but also when the disease progresses to fibrosis [90]. Therefore, the images are difficult to analyze and must be used in combination with perfusion imaging.

Chronic disease

CAD

CAD is the obstruction, damage or disease of arteries of the heart. Plaque buildup is characteristic of CAD and can cause narrowing and hardening of the large arteries in the heart slowing down blood flow. The most common cause of blockage is atherosclerosis, which will be discussed later. CAD is also called ischemic heart disease when there is inadequate blood supply to the heart causing ischemia. Prolonged ischemia can result in myocardial infarction or sudden death. PET imaging is used for the diagnosis, prognosis and risk stratification of CAD. A systematic review by Moudi et al. on the diagnosis of CAD by different imaging modalities concluded that PET has high diagnostic value based on sensitivity, specificity and accuracy [168].

PET imaging of MPI is used for detecting obstructive CAD by measuring flow-dependent tracer uptake and tracer accumulation, which is reflective of areas that have reduced blood flow [169]. Regions with decreased tracer uptake may be affected by atherosclerotic lesions or circulatory dysfunction. Visual comparison of stress and rest images may find: (i) normal myocardium which shows uniform radiotracer uptake at stress and rest; (ii) presence of ischemic myocardium where perfusion defects are seen on stress images, but not on rest images; (iii) presence of myocardial scarring where perfusion defects are seen in both at stress and rest images [170]. However, there are limitations with visual and semi-quantitative assessment of regional myocardial perfusion defects depending on the radiotracer chosen that may be overcome by absolute quantification with PET [171].

Absolute MBF in milliliters per gram per minute and coronary flow reserve (CFR) can be determined using dynamic imaging and emerge as a superior method to standard stress/rest imaging [172]. Static images alone have high sensitivity and accuracy but dynamic imaging provides additional diagnostic value by expanding the scope of PET to detect subclinical, non-obstructive CAD [11, 173-175]. Quantifying MBF or CFR can identify early functional abnormalities in circulation to detect precursors of CAD like early stages of atherosclerosis or microvascular dysfunction [176]. This is advantageous because functional abnormalities occur prior to structural alterations of the arterial wall commonly looked at for diagnosis [177]. MBF responses to vasomotor stress with the use of cold pressor testing or adenosine can be used for the identification of circulatory dysfunction and monitoring pharmacologic interventions or lifestyle modification whereas CFR has prognostic value [171, 172, 178]. CFR decreases in proportion to the degree of stenosis severity. With low-grade or absence of coronary stenosis, a reduced CFR reflects dysfunction of coronary microcirculation [179]. Patients with preserved CFR have a good prognosis for up to 3 years [176]. When perfusion defects appear, reduced CFR and LV dysfunction are linked to worse outcomes like adverse cardiac events and cardiac death [176, 180]. LV ejection fraction reserve has been shown to have prognostic value as well [181]. Cardiac PET with ^{14}N-ammonia or ^{82}Rubidium can assess regional MBF of the LV [171]. In subclinical CAD, there may be heterogeneous relative myocardial uptake of radiotracer or impaired hyperemic blood flow of the left ventricular myocardium [171]. There is great clinical potential when measuring MBF and CFR but there are several limitations that need to be recognized. Cut-off values or reference values for absolute perfusion need to be studied for various tracers and more information is needed about expected MBF and CFR values in different subpopulations.

Metabolic imaging of myocardial ischemia can be used in patients with known or suspected CAD to measure tissue viability. Obstruction of coronary arteries slows down or blocks blood flow in the heart causing ischemia. Under mild to moderate myocardial ischemia, oxygen deprivation leads to a decline in fatty acid oxidation while glucose metabolism increases [182]. This substrate switch ensures the continuation of energy production and cell survival. If there is no metabolic adaptation or ischemia is sustained and severe, cell death occurs by either apoptosis or necrosis [183]. With PET, ^{18}F-FDG uptake reflects metabolically active and viable myocardium capable of glucose utilization. ^{11}C-acetate can determine the amount of oxidative phosphorylation in cardiomyocytes and predict functional recovery after revascularization [184]. Depending on which myocardial metabolic pathways are still intact, viable myocardium can be detected and patients who would benefit from revascularization can be identified.

Atherosclerosis

Atherosclerosis is a disease of the arteries where accumulation of lipids and fibrous elements build up creating plaques (lesions). It begins with vascular endothelial dysfunction and can lead to heart disease and stroke if the plaque ruptures. Atherosclerosis develops over years, with a long subclinical period and can be the primary cause of coronary artery disease. Metabolic disorders also contribute to the development of atherosclerosis (discussed below) [185, 186]. As detailed by Evans et al. (2016), PET has several roles in assessing and monitoring atherosclerosis including detecting and quantifying inflammation in plaque by macrophages, detecting destabilizing plaque, and monitoring progression of therapy [5, 187, 188]. Inflammation, characterized by the recruitment of pro- and anti-inflammatory macrophages, and phagocytic cells to sites of injury or infection, is present at all stages of atherosclerosis from early plaque development to progression and rupture. Atherosclerosis has a long subclinical period where detection of underlying factors including inflammation, hypoxia and apoptosis would be useful before they develop into severe cases of disease.

PET imaging with ^{18}F-FDG has been used to assess inflammation caused by atherosclerosis as areas of inflammation are abundant in macrophages that have increased glycolytic activity and therefore have higher uptake of FDG. This provides improved specificity for determining local inflammation compared to measuring circulating biomarkers. However, ^{18}F-FDG is a non-specific marker for inflammation in atherosclerosis. Several other PET tracers have been evaluated for specific uptake that may be better suited for cardiac imaging of atherosclerosis including SSTR ligands and translocator protein ligands [189, 190]. These probes focus on identification of atherosclerosis after the subclinical period targeting biomarkers of vulnerable plaque to identify them prior to rupture.

Microcalcification occurs in response to inflammation and can cause increased mechanical wall stress and microfractures that lead to rupture of plaque. It can also be an indicator of accelerated atherosclerosis [191]. In atherosclerotic plaque, macrophages promote osteogenesis causing vascular calcification [192]. ^{18}F-NaF accumulation may be identifiable in areas of microcalcification in coronary arteries before structural coronary artery calcification in the advanced stages of CAD detected with CT [192-194]. Uptake of this tracer in the heart is low but early detection and quantification of molecular changes in atherosclerotic plaque have been noted in the heart, specifically the aorta [194]. Similarly, ^{18}F-fluoride accumulates in regions of active microcalcification observed during the early stages of plaque formation. It has shown promising characteristics as a probe for detecting vulnerable plaque with highly specific accumulation, low background activity, and easy accessibility [194].

Hypoxia has known involvement in atherogenesis and has led to the development of PET probes for molecular imaging of hypoxia in plaque [195]. Hypoxia may be indicative of vulnerable plaques. There is limited literature on PET imaging of atherosclerotic hypoxia in humans. However, ^{18}F-fluoromisonidazole (FMISO) has been used to identify hypoxia in advanced atherosclerotic plaque in rabbits [39]. Regions with known atherosclerotic plaque had higher uptake than normal regions. Further investigation is needed into the potential usefulness of this probe in humans.

Cardiac myocyte apoptosis is an underlying factor in the development and progression of atherosclerosis [196, 197]. Early identification of apoptosis can prevent scar tissue build up and reduce loss of heart function. There are two pathways that lead to apoptosis: extrinsic or intrinsic [198]. Annexin V is a protein in the intrinsic pathway of apoptosis that binds with high affinity to phosphatidylserine present on the surface of apoptotic cells [199, 200]. Novel ^{18}F labeled peptides that target protein Annexin V have been continuously developed in an attempt to improve retention and tissue uptake compared to background uptake and blood [200-202]. These tracers that target Annexin V bind not only to apoptotic cells but necrotic cells as well requiring additional testing [200]. There is a need for the development of a radiotracer that can be used with PET for specific, accurate and early identification of apoptosis.

Impaired glucose metabolism

Metabolic abnormalities like impaired glucose metabolism are associated with increased risk of cardiac pathology. Impaired glucose tolerance (IGT) and insulin resistance (IR) can lead to the development of type 2 diabetes mellitus (DM) and metabolic syndrome. IGT is a state of hyperglycemia that can increase the risk of cardiovascular complications [203]. There appears to be a two-way relationship between impaired glucose metabolism and adverse cardiac events [204]. Impaired glucose metabolism is a risk factor for cardiovascular disease while in some cases, heart failure occurs first followed by impaired glucose metabolism that eventually leads to the development of type 2 DM [203, 204]. Abnormal glucose metabolism often goes undetected if individuals have no symptoms [204]. PET imaging has been used to detect subclinical metabolic changes and changes in blood flow in the heart before advanced stages of disease.

Patients with IGT or type 2 DM have been found to be at an increased risk for development of atherosclerosis. Mechanisms between atherosclerosis and type 2 DM are unknown but atherosclerosis remains a major cause of morbidity and mortality in the diabetic population [205, 206]. As mentioned in the previous section, an early sign of atherosclerosis is vascular inflammation, which can be detected and quantified by ^{18}F-FDG with PET imaging in diabetic and IGT patients [205, 207]. Similarly, ^{18}F-FDG has been used to identify inflammation involved in carotid atherosclerosis in patients with metabolic syndrome [208]. ^{18}F-FDG has also been used to track therapeutic benefits of pioglitazone, a peroxisome proliferator-activated receptor gamma agonists [209, 210]. Pioglitazone is used as a treatment for type 2 DM to improve IR but may also be useful in reducing atherosclerotic inflammation [209, 211, 212]. A study by Nitta et al. suggests that pioglitazone may protect against cardiac events in patients with IGT or type 2 DM by suppressing coronary inflammation [210].

Changes in cardiac metabolism towards fatty acid metabolism may also contribute to the development of heart disease. Abnormal fatty acid metabolism plays a role in the development of IR and disruption of glucose homeostasis [213]. PET imaging with ^{11}C-palmitate has been used to assess myocardial fatty acid metabolism in the heart in individuals with type 2 DM and IGT [214, 215]. More recently, a positron-emitting fatty acid analog, 14(*R*,*S*)-[^{18}F] fluoro-6-thia-heptadecanoic acid (FTHA), was developed and used to image and assess organ-specific partitioning of dietary fatty acids with PET/CT [216]. The tracer is administered orally with a meal and becomes trapped in the heart mitochondria after undergoing the initial steps of beta-oxidation. In rats and humans with IGT, an increase in myocardial dietary fatty acid uptake was noted [217-219]. It has been suggested that increased myocardial uptake of dietary fatty acids may be an early marker or potential contributor to myocardial dysfunction associated with prediabetes and diabetes [217]. Increased myocardial fatty acid partitioning is also associated with early impairment in left ventricular systolic and diastolic functions plus increased cardiac oxidative metabolism suggesting a possible role in the development of metabolic cardiomyopathy [218].

Patients with IGT have significantly reduced left ventricular stroke volume and ejection fraction and tend to display impaired diastolic function, as assessed by PET ventriculography all of which are related to diabetic cardiomyopathy. Early left ventricular function impairment and increased myocardial oxidative metabolism have been found to be associated with excessive myocardial partitioning of dietary fatty acids [218]. PET imaging with ^{11}C-acetate has

shown that patients with impaired glucose metabolism have an increase in myocardial oxygen consumption [218]. Additionally, PET has been used to identify coronary dysfunction by measuring MBF in patients with impaired glucose metabolism [214, 220, 221]. Coronary circulatory function was also found to decrease as severity of IR and carbohydrate metabolism increase [220].

Inflammation tracer development

With any type of molecular imaging, there is importance in identifying and quantifying disease before it advances to the point that therapeutic intervention is no longer effective. This article has touched on a variety of PET tracers used for detecting cardiac diseases. Detecting inflammation is common amongst the diseases mentioned. ^{18}F-FDG is used widely to measure inflammation by tracking macrophage glycolytic activity; however, it has several limitations that hinder its ability to accurately detect activated macrophages. The lack of specificity allows this probe to target other immune cells as well. A recently published article briefly mentions alternative radiotracers and targets to ^{18}F-FDG that are currently in development for specific cardiac diseases [222]. Select radiotracers that have tested in animals and those with potential to be developed to image inflammation in the heart are reviewed here in more detail.

^{68}Ga-NODAGA-RGD is a peptide tracer targeting integrin $\alpha_v\beta_3$ expressed on macrophages and myofibroblasts involved in extracellular matrix remodeling. It was first used to study $\alpha_v\beta_3$ expressed on activated endothelial cells involved in tumor growth, invasiveness, and metastasis [223, 224]. ^{68}Ga-NODAGA-RGD was tested in pigs with induced flow-limiting coronary stenosis to study the effects of flow-limiting coronary stenosis on expression of integrin $\alpha_v\beta_3$ [225]. The study compared $\alpha_v\beta_3$ expression in ischemic versus non-ischemic myocardium and viable versus injured ischemic myocardial areas two weeks after induction of coronary stenosis in pigs. ^{68}Ga-NODAGA-RGD PET imaging was used in combination with ^{15}O-water perfusion PET, and histological evaluation of myocardial injury to compare $\alpha_v\beta_3$ expression in ischemic versus non-ischemic myocardium and viable versus injured ischemic myocardial areas two weeks after induction of coronary stenosis in pigs. The tracer localized in irreversibly injured myocardium, and not viable myocardium. ^{68}Ga-NODAGA-RGD may be useful for the identification of $\alpha_v\beta_3$ integrin activation associated with repair of myocardial injury.

^{18}F-Macroflor is polyglucose nanoparticle that has been shrunken in size to allow rapid renal excretion. Nanoparticles are internalized by phagocytic myeloid cells suggesting a promising strategy for imaging cardiac macrophages. ^{18}F-Macroflor, using integrated PET imaging, was tested in mice, rabbits, and a non-human primate and found to have high affinity for macrophages residing in cardiovascular organs [226]. ^{18}F-Macroflor undergoes rapid clearance from blood pool (6.5 minutes in mice, 22 minutes in rabbits, 21.7 minutes in non-human primates) into macrophages with time to be imaged before the tracer is excreted. Uptake was significantly increased in mice with atherosclerosis imaged with PET/CT. When compared to ^{18}F-FDG uptake in rabbits with atherosclerosis, there was an overlap between the tracers. However, ^{18}F-Macroflor had negligible myocyte uptake which is beneficial for cardiac inflammation imaging. Increased specificity for macrophages and rapid pharmacokinetics suggest ^{18}F-Macroflor is a promising cardiac inflammation imaging radiotracer but further research is required in non-human primates prior to human studies.

A promising alternative has been developed that may be more specific in targeting inflammation than ^{18}F-FDG. Phenix et al. developed a method for synthesizing an analogue of ^{18}F-FDG using an enzymatic approach for tagging acid *β*-glucocerebrosidase (GCase), a recombinant enzyme formulated in commercial Cerezyme which is used to treat Gaucher disease [227]. ^{18}F-Cerezyme was obtained in a total synthesis time of about 2.5 hours and is derived from ^{18}F-FDG. Phenix et al. provides animal testing of this tracer in which they examined the biodistribution of GCase in mice. ^{18}F-Cerezyme has high affinity for mannose receptors on macrophages and showed the highest uptake in macrophage-rich organs (e.g., liver and spleen). Uptake was also seen in the gall bladder, kidneys, intestines, heart, and femur. The biodistribution and PET imaging

studies on animals suggest that ^{18}F-Cerezyme is a novel powerful tool for monitoring enzyme distribution. The study concluded that the ^{18}F-labeling method could be adapted for use of alternative enzymes, and create opportunities for application to a variety of enzyme replacement therapies. However, ability to detect macrophage infiltration in cardiac tissue could be utilized as a more specific alternative to ^{18}F-FDG to detect inflammation. Thus, this radiotracer appears promising but requires further investigation.

Developing a PET probe that targets enzyme activity of macrophages or subpopulations of macrophages, like the pro-inflammatory response of M1 or the anti-inflammatory response of M2, will improve the diagnostic capabilities of PET imaging. In reviews by Ali et al. and Quillard et al., the targeting of macrophage enzymatic activity of proteases that participate in extracellular matrix remodeling are discussed. Specifically, metalloproteinases and cysteine cathepsins, as well as targeting myeloperoxidase activity of macrophages [228, 229]. Metalloproteinases switch from M1 to M2 macrophages with disease progression leading to difficulties in choosing a target subpopulation unless the time of disease onset is known [230]. Cathepsins K, S, L, and B are suggested to play a role in cardiovascular disease but some cysteine cathepsins like B, L and H are expressed in most immune cells and tissues [231, 232]. One study suggests cathepsins Z and F may be exclusive to macrophages after comparison to dendritic cells and splenocytes and are involved in antigen processing and presentation [233]. However, a review by Riese et al., classifies both cathepsin F and Z as having widespread distribution [234].

Both cysteine cathepsins and MMP's have potential to differentiate between macrophages and other immune cells with PET imaging but no tracer exists that has high specificity for macrophage subpopulations and since myeloperoxidase is secreted by both neutrophils and macrophages it is not the best option if looking for inflammation caused only by macrophages. Protease imaging utilizes small molecules that bind to specific pockets usually within the active site of the protein. Alternatively, radiotracers can be mimics of protease substrates that are hydrolyzed by the enzyme. An enzyme targeting tracer that becomes trapped within the active site of an enzyme be of value for macrophage-specific imaging. Imaging of macrophage enzyme activity holds promise for cardiac inflammation detection but requires further research and refinement before use in the clinical settings for reliable diagnosis and prognosis of cardiac disease.

Disclosure of conflict of interest

None.

Address correspondence to: Dr. Simon J Lees, Medical Sciences Division, Northern Ontario School of Medicine, Lakehead University, Thunder Bay, Ontario, Canada. E-mail: simon.lees@nosm.ca

References

[1] Schelbert HR. Positron emission tomography measurements of myocardial blood flow: assessing coronary circulatory function and clinical implications. Heart Br Card Soc 2012; 98: 592-600.

[2] Ziadi MC, Dekemp RA, Williams KA, Guo A, Chow BJ, Renaud JM, Ruddy TD, Sarveswaran N, Tee RE, Beanlands RS. Impaired myocardial flow reserve on rubidium-82 positron emission tomography imaging predicts adverse outcomes in patients assessed for myocardial ischemia. J Am Coll Cardiol 2011; 58: 740-748.

[3] Osterholt M, Sen S, Dilsizian V and Taegtmeyer H. Targeted metabolic imaging to improve the management of heart disease. JACC Cardiovasc Imaging 2012; 5: 214-226.

[4] Peterson LR and Gropler RJ. Radionuclide imaging of myocardial metabolism. Circ Cardiovasc Imaging 2010; 3: 211-222.

[5] Evans NR, Tarkin JM, Chowdhury MM, Warburton EA, Rudd JH. PET imaging of atherosclerotic disease: advancing plaque assessment from anatomy to pathophysiology. Curr Atheroscler Rep 2016; 18: 30.

[6] Tarkin JM, Joshi FR, Evans NR, Chowdhury MM, Figg NL, Shah AV, Starks LT, Martin-Garrido A, Manavaki R, Yu E, Kuc RE, Grassi L, Kreuzhuber R, Kostadima MA, Frontini M, Kirkpatrick PJ, Coughlin PA, Gopalan D, Fryer TD, Buscombe JR, Groves AM, Ouwehand WH, Bennett MR, Warburton EA, Davenport AP and Rudd JH. Detection of atherosclerotic inflammation by 68Ga-DOTATATE PET compared to [18F]FDG PET imaging. J Am Coll Cardiol 2017; 69: 1774-1791.

[7] Cerqueira MD, Allman KC, Ficaro EP, Hansen CL, Nichols KJ, Thompson RC, Van Decker WA and Yakovlevitch M. Recommendations for reducing radiation exposure in myocardial perfu-

sion imaging. J Nucl Cardiol 2010; 17: 709-718.
[8] Timothy M Bateman, Heller GV, McGhie AI, Friedman JD, Case JA, Bryngelson JR, Hertenstein GK, Moutray KL, Reid K and Cullom SJ. Diagnostic accuracy of rest/stress ECG-gated Rb-82 myocardial perfusion PET: comparison with ECG-gated Tc-99m sestamibi SPECT. J Nucl Cardiol 2006; 13: 24-33.
[9] Blankenstein J, McArdle B, Small G, Guo A, Garrard L, Chow B, Ruddy T, Wells G, Beanlands R and deKemp R. Reduced rate of diagnostic coronary imaging following rubidium PET vs thallium SPECT, as alternatives to technetium SPECT myocardial perfusion imaging. J Nucl Med 2013; 54 Suppl 2: 1735.
[10] Merhige ME, Breen WJ, Shelton V, Houston T, D'Arcy BJ and Perna AF. Impact of myocardial perfusion imaging with PET and (82)Rb on downstream invasive procedure utilization, costs, and outcomes in coronary disease management. J Nucl Med 2007; 48: 1069-1076.
[11] Mylonas I, Kazmi M, Fuller L, deKemp RA, Yam Y, Chen L, Beanlands RS and Chow BJ. Measuring coronary artery calcification using positron emission tomography-computed tomography attenuation correction images. Eur Heart J Cardiovasc Imaging 2012; 13: 786-792.
[12] Namdar M, Hany TF, Koepfli P, Siegrist PT, Burger C, Wyss CA, Luscher TF, von Schulthess GK and Kaufmann PA. Integrated PET/CT for the assessment of coronary artery disease: a feasibility study. J Nucl Med 2005; 46: 930-935.
[13] Leide-Svegborn S. Radiation exposure of patients and personnel from a PET/CT procedure with 18F-FDG. Radiat Prot Dosimetry 2010; 139: 208-213.
[14] Nensa F, Poeppel TD, Beiderwellen K, Schelhorn J, Mahabadi AA, Erbel R, Heusch P, Nassenstein K, Bockisch A, Forsting M and Schlosser T. Hybrid PET/MR imaging of the heart: feasibility and initial results. Radiology 2013; 268: 366-373.
[15] Chen K and Chen X. Design and development of molecular imaging probes. Curr Top Med Chem 2010; 10: 1227-1236.
[16] Alva-Sánchez H, Quintana-Bautista C, Martínez-Dávalos A, Ávila-Rodríguez MA and Rodríguez-Villafuerte M. Positron range in tissue-equivalent materials: experimental microPET studies. Phys Med Biol 2016; 61: 6307-6321.
[17] Phelps ME, Hoffman EJ, Huang SC and Ter-Pogossian MM. Effect of positron range on spatial resolution. J Nucl Med 1975; 16: 649-652.
[18] Senthamizhchelvan S, Bravo PE, Esaias C, Lodge MA, Merrill J, Hobbs RF, Sgouros G and Bengel FM. Human biodistribution and radiation dosimetry of 82Rb. J Nucl Med 2010; 51: 1592-1599.
[19] Knaapen P, de Haan S, Hoekstra OS, Halbmeijer R, Appelman YE, Groothuis JG, Comans EF, Meijerink MR, Lammertsma AA, Lubberink M, Götte MJ, van Rossum AC. Cardiac PET-CT: advanced hybrid imaging for the detection of coronary artery disease. Neth Heart J 2010; 18: 90-98.
[20] Krivokapich J, Smith GT, Huang SC, Hoffman EJ, Ratib O, Phelps ME and Schelbert HR. 13N ammonia myocardial imaging at rest and with exercise in normal volunteers. Quantification of absolute myocardial perfusion with dynamic positron emission tomography. Circulation 1989; 80: 1328-1337.
[21] Chow BJ, Beanlands RS, Lee A, DaSilva JN, deKemp RA, Alkahtani A and Ruddy TD. Treadmill exercise produces larger perfusion defects than dipyridamole stress N-13 ammonia positron emission tomography. J Am Coll Cardiol 2006; 47: 411-416.
[22] Abramson BL, Ruddy TD, deKemp RA, Laramee LA, Marquis JF and Beanlands RS. Stress perfusion/metabolism imaging: a pilot study for a potential new approach to the diagnosis of coronary disease in women. J Nucl Cardiol 2000; 7: 205-212.
[23] Wyss CA, Koepfli P, Mikolajczyk K, Burger C, von Schulthess GK and Kaufmann PA. Bicycle exercise stress in PET for assessment of coronary flow reserve: repeatability and comparison with adenosine stress. J Nucl Med 2003; 44: 146-154.
[24] Botvinick EH. Current methods of pharmacologic stress testing and the potential advantages of new agents. J Nucl Med Technol 2009; 37: 14-25.
[25] Geleijnse ML, Elhendy A, Fioretti PM and Roelandt JR. Dobutamine stress myocardial perfusion imaging. J Am Coll Cardiol 2000; 36: 2017-2027.
[26] Leppo JA. Dipyridamole myocardial perfusion imaging. J Nucl Med 1994; 35: 730-733.
[27] Bateman TM. Cardiac positron emission tomography and the role of adenosine pharmacologic stress. Am J Cardiol 2004; 94: 19D-24D; discussion 24D-25D.
[28] Buhr C, Gössl M, Erbel R and Eggebrecht H. Regadenoson in the detection of coronary artery disease. Vasc Health Risk Manag 2008; 4: 337-340.
[29] Michiels C. Physiological and pathological responses to hypoxia. Am J Pathol 2004; 164: 1875-1882.
[30] Lee ST and Scott AM. Hypoxia positron emission tomography imaging with ^{18}F-fluoromisonidazole. Semin Nucl Med 2007; 37: 451-461.

[31] Kobayashi H, Hirata K, Yamaguchi S, Terasaka S, Shiga T and Houkin K. Usefulness of FMISO-PET for glioma analysis. Neurol Med Chir (Tokyo) 2013; 53: 773-778.
[32] Handley MG, Medina RA, Mariotti E, Kenny GD, Shaw KP, Yan R, Eykyn TR, Blower PJ and Southworth R. Cardiac hypoxia imaging: second-generation analogues of 64Cu-ATSM. J Nucl Med 2014; 55: 488-494.
[33] Whitmore GF and Varghese AJ. The biological properties of reduced nitroheterocyclics and possible underlying biochemical mechanisms. Biochem Pharmacol 1986; 35: 97-103.
[34] Yang DJ, Wallace S, Cherif A, Li C, Gretzer MB, Kim EE and Podoloff DA. Development of F-18-labeled fluoroerythronitroimidazole as a PET agent for imaging tumor hypoxia. Radiology 1995; 194: 795-800.
[35] Arabi M and Piert M. Hypoxia PET/CT imaging: implications for radiation oncology. Q J Nucl Med Mol Imaging 2010; 54: 500-509.
[36] Troost EG, Laverman P, Kaanders JH, Philippens M, Lok J, Oyen WJ, van der Kogel AJ, Boerman OC and Bussink J. Imaging hypoxia after oxygenation-modification: comparing [18F]FMISO autoradiography with pimonidazole immunohistochemistry in human xenograft tumors. Radiother Oncol 2006; 80: 157-164.
[37] Nunn A, Linder K and Strauss HW. Nitroimidazoles and imaging hypoxia. Eur J Nucl Med 1995; 22: 265-280.
[38] Rademakers SE, Lok J, van der Kogel AJ, Bussink J and Kaanders JH. Metabolic markers in relation to hypoxia; staining patterns and colocalization of pimonidazole, HIF-1α, CAIX, LDH-5, GLUT-1, MCT1 and MCT4. BMC Cancer 2011; 11: 167.
[39] Mateo J, Izquierdo-Garcia D, Badimon JJ, Fayad ZA and Fuster V. Noninvasive assessment of hypoxia in rabbit advanced atherosclerosis using ^{18}F-fluoromisonidazole positron emission tomographic imaging. Circ Cardiovasc Imaging 2014; 7: 312-320.
[40] Laurens E, Yeoh SD, Rigopoulos A, Cao D, Cartwright GA, O'Keefe GJ, Tochon-Danguy HJ, White JM, Scott AM and Ackermann U. Radiolabelling and evaluation of a novel sulfoxide as a PET imaging agent for tumor hypoxia. Nucl Med Biol 2014; 41: 419-425.
[41] Martin GV, Caldwell JH, Graham MM, Grierson JR, Kroll K, Cowan MJ, Lewellen TK, Rasey JS, Casciari JJ and Krohn KA. Noninvasive detection of hypoxic myocardium using fluorine-18-fluoromisonidazole and positron emission tomography. J Nucl Med 1992; 33: 2202-2208.
[42] Caldwell JH, Revenaugh JR, Martin GV, Johnson PM, Rasey JS and Krohn KA. Comparison of fluorine-18-fluorodeoxyglucose and tritiated fluoromisonidazole uptake during low-flow ischemia. J Nucl Med 1995; 36: 1633-1638.
[43] Takasawa M, Moustafa RR and Baron JC. Applications of nitroimidazole in vivo hypoxia imaging in ischemic stroke. Stroke 2008; 39: 1629-1637.
[44] Silvola JM, Saraste A, Forsback S, Laine VJ, Saukko P, Heinonen SE, Ylä-Herttuala S, Roivainen A and Knuuti J. Detection of hypoxia by [18F]EF5 in atherosclerotic plaques in mice. Arterioscler Thromb Vasc Biol 2011; 31: 1011-1015.
[45] Peeters SG, Zegers CM, Lieuwes NG, van Elmpt W, Eriksson J, van Dongen GA, Dubois L and Lambin P. A comparative study of the hypoxia PET tracers [^{18}F]HX4, [^{18}F]FAZA, and [^{18}F]FMISO in a preclinical tumor model. Int J Radiat Oncol Biol Phys 2015; 91: 351-359.
[46] Wack LJ, Mönnich D, van Elmpt W, Zegers CM, Troost EG, Zips D and Thorwarth D. Comparison of [18F]-FMISO, [18F]-FAZA and [18F]-HX4 for PET imaging of hypoxia--a simulation study. Acta Oncol Stockh Swed 2015; 54: 1370-1377.
[47] Reischl G, Dorow DS, Cullinane C, Katsifis A, Roselt P, Binns D and Hicks RJ. Imaging of tumor hypoxia with [124I]IAZA in comparison with [18F]FMISO and [18F]FAZA--first small animal PET results. J Pharm Pharm Sci 2007; 10: 203-211.
[48] Li L, Hu M, Zhu H, Zhao W, Yang G and Yu J. Comparison of 18F-Fluoroerythronitroimidazole and 18F-fluorodeoxyglucose positron emission tomography and prognostic value in locally advanced non-small-cell lung cancer. Clin Lung Cancer 2010; 11: 335-340.
[49] van der Valk FM, Sluimer JC, Vöö SA, Verberne HJ, Nederveen AJ, Windhorst AD, Stroes ES, Lambin P and Daemen MJ. In vivo imaging of hypoxia in atherosclerotic plaques in humans. JACC Cardiovasc Imaging 2015; 8: 1340-1341.
[50] Bourgeois M, Rajerison H, Guerard F, Mougin-Degraef M, Barbet J, Michel N, Cherel M and Faivre-Chauvet A. Contribution of [64Cu]-ATSM PET in molecular imaging of tumour hypoxia compared to classical [18F]-MISO--a selected review. Nucl Med Rev Cent East Eur 2011; 14: 90-95.
[51] Vāvere AL and Lewis JS. Cu-ATSM: a radiopharmaceutical for the PET imaging of hypoxia. Dalton Trans Camb Engl 2003 2007; 4893-4902.
[52] Lewis JS, Herrero P, Sharp TL, Engelbach JA, Fujibayashi Y, Laforest R, Kovacs A, Gropler RJ and Welch MJ. Delineation of hypoxia in canine myocardium using PET and copper(II)-diacetyl-bis(N(4)-methylthiosemicarbazone). J Nucl Med 2002; 43: 1557-1569.
[53] Obata A, Kasamatsu S, McCarthy DW, Welch MJ, Saji H, Yonekura Y and Fujibayashi Y. Pro-

duction of therapeutic quantities of (64)Cu using a 12 MeV cyclotron. Nucl Med Biol 2003; 30: 535-539.
[54] Dearling JL and Packard AB. Some thoughts on the mechanism of cellular trapping of Cu(II)-ATSM. Nucl Med Biol 2010; 37: 237-243.
[55] Holland JP, Lewis JS and Dehdashti F. Assessing tumor hypoxia by positron emission tomography with Cu-ATSM. Q J Nucl Med Mol Imaging 2009; 53: 193-200.
[56] Dearling JL, Lewis JS, Mullen GE, Welch MJ and Blower PJ. Copper bis (thiosemicarbazone) complexes as hypoxia imaging agents: structure-activity relationships. J Biol Inorg Chem 2002; 7: 249-259.
[57] Dearling JL, Lewis JS, Mullen GE, Rae MT, Zweit J and Blower PJ. Design of hypoxia-targeting radiopharmaceuticals: selective uptake of copper-64 complexes in hypoxic cells in vitro. Eur J Nucl Med 1998; 25: 788-792.
[58] Maurer RI, Blower PJ, Dilworth JR, Reynolds CA, Zheng Y and Mullen GE. Studies on the mechanism of hypoxic selectivity in copper bis (thiosemicarbazone) radiopharmaceuticals. J Med Chem 2002; 45: 1420-1431.
[59] Takahashi N, Fujibayashi Y, Yonekura Y, Welch MJ, Waki A, Tsuchida T, Sadato N, Sugimoto K, Nakano A, Lee JD and Itoh H. Copper-62 ATSM as a hypoxic tissue tracer in myocardial ischemia. Ann Nucl Med 2001; 15: 293-296.
[60] Medina RA, Mariotti E, Pavlovic D, Shaw KP, Eykyn TR, Blower PJ and Southworth R. 64Cu-CTS: a promising radiopharmaceutical for the identification of low-grade cardiac hypoxia by PET. J Nucl Med 2015; 56: 921-926.
[61] Sun D, Nguyen N, DeGrado TR, Schwaiger M and Brosius FC. Ischemia induces translocation of the insulin-responsive glucose transporter GLUT4 to the plasma membrane of cardiac myocytes. Circulation 1994; 89: 793-798.
[62] Brosius FC, Liu Y, Nguyen N, Sun D, Bartlett J and Schwaiger M. Persistent myocardial ischemia increases GLUT1 glucose transporter expression in both ischemic and non-ischemic heart regions. J Mol Cell Cardiol 1997; 29: 1675-1685.
[63] Libby P. Inflammation and cardiovascular disease mechanisms. Am J Clin Nutr 2006; 83: 456S-460S.
[64] Kaim AH, Weber B, Kurrer MO, Gottschalk J, Von Schulthess GK and Buck A. Autoradiographic quantification of 18F-FDG uptake in experimental soft-tissue abscesses in rats. Radiology 2002; 223: 446-451.
[65] Kubota R, Kubota K, Yamada S, Tada M, Ido T and Tamahashi N. Microautoradiographic study for the differentiation of intratumoral macrophages, granulation tissues and cancer cells by the dynamics of fluorine-18-fluorodeoxyglucose uptake. J Nucl Med 1994; 35: 104-112.
[66] Deichen JT, Prante O, Gack M, Schmiedehausen K and Kuwert T. Uptake of [18F]fluorodeoxyglucose in human monocyte-macrophages in vitro. Eur J Nucl Med Mol Imaging 2003; 30: 267-273.
[67] Randle PJ, England PJ and Denton RM. Control of the tricarboxylate cycle and its interactions with glycolysis during acetate utilization in rat heart. Biochem J 1970; 117: 677-695.
[68] Klein LJ, Visser FC, Nurmohamed SA, Vink A, Peters JH, Knaapen P, Kruijer PS, Herscheid JD, Teule GJ and Visser CA. Feasibility of planar myocardial carbon 11-acetate imaging. J Nucl Cardiol 2000; 7: 221-227.
[69] Gropler RJ, Siegel BA and Geltman EM. Myocardial uptake of carbon-11-acetate as an indirect estimate of regional myocardial blood flow. J Nucl Med 1991; 32: 245-251.
[70] Lear JL. Relationship between myocardial clearance rates of carbon-11-acetate-derived radiolabel and oxidative metabolism: physiologic basis and clinical significance. J Nucl Med 1991; 32: 1957-1960.
[71] Brown M, Marshall DR, Sobel BE and Bergmann SR. Delineation of myocardial oxygen utilization with carbon-11-labeled acetate. Circulation 1987; 76: 687-696.
[72] Grassi I, Nanni C, Allegri V, Morigi JJ, Montini GC, Castellucci P and Fanti S. The clinical use of PET with (11)C-acetate. Am J Nucl Med Mol Imaging 2012; 2: 33-47.
[73] Sun KT, Yeatman LA, Buxton DB, Chen K, Johnson JA, Huang SC, Kofoed KF, Weismueller S, Czernin J, Phelps ME and Schelbert HR. Simultaneous measurement of myocardial oxygen consumption and blood flow using [1-carbon-11]acetate. J Nucl Med 1998; 39: 272-280.
[74] Wolpers HG, Burchert W, van den Hoff J, Weinhardt R, Meyer GJ and Lichtlen PR. Assessment of myocardial viability by use of ^{11}C-acetate and positron emission tomography. Threshold criteria of reversible dysfunction. Circulation 1997; 95: 1417-1424.
[75] Timmer SA, Lubberink M, Germans T, Götte MJ, ten Berg JM, ten Cate FJ, van Rossum AC, Lammertsma AA, and Knaapen P. Potential of [11C]acetate for measuring myocardial blood flow: studies in normal subjects and patients with hypertrophic cardiomyopathy. J Nucl Cardiol 2010; 17: 264-275.
[76] Sörensen J, Valind S, and Andersson LG. Simultaneous quantification of myocardial perfusion, oxidative metabolism, cardiac efficiency and pump function at rest and during supine bicycle exercise using 1-11C-acetate PET–a pi-

lot study. Clin Physiol Funct Imaging 2010; 30: 279-284.
[77] Bergmann SR, Weinheimer CJ, Markham J and Herrero P. Quantitation of myocardial fatty acid metabolism using PET. J Nucl Med 1996; 37: 1723-1730.
[78] Kisrieva-Ware Z, Coggan AR, Sharp TL, Dence CS, Gropler RJ and Herrero P. Assessment of myocardial triglyceride oxidation with PET and 11C-palmitate. J Nucl Cardiol 2009; 16: 411-421.
[79] Tamaki N, Fujibayashi Y, Magata Y, Yonekura Y and Konishi J. Radionuclide assessment of myocardial fatty acid metabolism by PET and SPECT. J Nucl Cardiol 1995; 2: 256-266.
[80] Tamaki N, Morita K, Kuge Y and Tsukamoto E. The role of fatty acids in cardiac imaging. J Nucl Med 2000; 41: 1525-1534.
[81] Fox KA, Abendschein DR, Ambos HD, Sobel BE and Bergmann SR. Efflux of metabolized and nonmetabolized fatty acid from canine myocardium. Implications for quantifying myocardial metabolism tomographically. Circ Res 1985; 57: 232-243.
[82] Li Y, Huang T, Zhang X, Zhong M, Walker NN, He J, Berr SS, Keller SR and Kundu BK. Determination of fatty acid metabolism with dynamic [11C]Palmitate positron emission tomography of mouse heart in vivo. Mol Imaging 2015; 14: 516-525.
[83] Nuyts H, Maes A, Vrolix M, Schiepers C, Schelbert H, Kuhle W, Bormans G, Poppe G, Buxton D, Suetens P, De Geest H and Mortelmans L. Three-dimensional correction for spillover and recovery of myocardial PET images. J Nucl Med 1996; 37: 767-774.
[84] Blankstein R, Osborne M, Naya M, Waller A, Kim CK, Murthy VL, Kazemian P, Kwong RY, Tokuda M, Skali H, Padera R, Hainer J, Stevenson WG, Dorbala S and Di Carli MF. Cardiac positron emission tomography enhances prognostic assessments of patients with suspected cardiac sarcoidosis. J Am Coll Cardiol 2014; 63: 329-336.
[85] Pessin JE and Bell GI. Mammalian facilitative glucose transporter family: structure and molecular regulation. Annu Rev Physiol 1992; 54: 911-930.
[86] Iozzo P, Geisler F, Oikonen V, Mäki M, Takala T, Solin O, Ferrannini E, Knuuti J, Nuutila P; 18F-FDG PET Study. Insulin stimulates liver glucose uptake in humans: an 18F-FDG PET study. J Nucl Med 2003; 44: 682-689.
[87] Garbarino S, Vivaldi V, Delbary F, Caviglia G, Piana M, Marini C, Capitanio S, Calamia I, Buschiazzo A and Sambuceti G. A new compartmental method for the analysis of liver FDG kinetics in small animal models. EJNMMI Res 2015; 5: 107.
[88] Iozzo P, Chareonthaitawee P, Di Terlizzi M, Betteridge DJ, Ferrannini E and Camici PG. Regional myocardial blood flow and glucose utilization during fasting and physiological hyperinsulinemia in humans. Am J Physiol Endocrinol Metab 2002; 282: E1163-1171.
[89] Kumar P, Patel CD, Singla S and Malhotra A. Effect of duration of fasting and diet on the myocardial uptake of F-18-2-fluoro-2-deoxyglucose (F-18 FDG) at rest. Indian J Nucl Med 2014; 29: 140-145.
[90] Skali H, Schulman AR and Dorbala S. 18F-FDG PET/CT for the assessment of myocardial sarcoidosis. Curr Cardiol Rep 2013; 15: 352.
[91] Chang JM, Lee HJ, Goo JM, Lee HY, Lee JJ, Chung JK, and Im JG. False positive and false negative FDG-PET scans in various thoracic diseases. Korean J Radiol 2006; 7: 57-69.
[92] Armani C, Catalani E, Balbarini A, Bagnoli P and Cervia D. Expression, pharmacology, and functional role of somatostatin receptor subtypes 1 and 2 in human macrophages. J Leukoc Biol 2007; 81: 845-855.
[93] Dalm VA, van Hagen PM, van Koetsveld PM, Achilefu S, Houtsmuller AB, Pols DH, van der Lely AJ, Lamberts SW, Hofland LJ. Expression of somatostatin, cortistatin, and somatostatin receptors in human monocytes, macrophages, and dendritic cells. Am J Physiol Endocrinol Metab 2003; 285: E344-353.
[94] Lichtenauer-Kaligis EG, van Hagen PM, Lamberts SW and Hofland LJ. Somatostatin receptor subtypes in human immune cells. Eur J Endocrinol 2000; 143 Suppl 1: S21-25.
[95] Adams RL, Adams IP, Lindow SW, Zhong W and Atkin SL. Somatostatin receptors 2 and 5 are preferentially expressed in proliferating endothelium. Br J Cancer 2005; 92: 1493-1498.
[96] McCarthy MJ, Loftus IM, Thompson MM, Jones L, London NJ, Bell PR, Naylor AR and Brindle NP. Angiogenesis and the atherosclerotic carotid plaque: an association between symptomatology and plaque morphology. J Vasc Surg 1999; 30: 261-268.
[97] Li X, Samnick S, Lapa C, Israel I, Buck AK, Kreissl MC and Bauer W. 68Ga-DOTATATE PET/CT for the detection of inflammation of large arteries: correlation with18F-FDG, calcium burden and risk factors. EJNMMI Res 2012; 2: 52.
[98] Reubi JC, Schär JC, Waser B, Wenger S, Heppeler A, Schmitt JS and Mäcke HR. Affinity profiles for human somatostatin receptor subtypes SST1-SST5 of somatostatin radiotracers selected for scintigraphic and radiotherapeutic use. Eur J Nucl Med 2000; 27: 273-282.
[99] Velikyan I, Sundin A, Sörensen J, Lubberink M, Sandström M, Garske-Román U, Lundqvist H, Granberg D and Eriksson B. Quantitative and

qualitative intrapatient comparison of 68Ga-DOTATOC and 68Ga-DOTATATE: net uptake rate for accurate quantification. J Nucl Med 2014; 55: 204-210.
[100] Banerjee SR and Pomper MG. Clinical applications of gallium-68. Appl Radiat Isot 2013; 76: 2-13.
[101] Velikyan I. Positron emitting [68Ga]Ga-based imaging agents: chemistry and diversity. Med Chem 2011; 7: 345-379.
[102] Zhernosekov KP, Filosofov DV, Baum RP, Aschoff P, Bihl H, Razbash AA, Jahn M, Jennewein M and Rösch F. Processing of generator-produced 68Ga for medical application. J Nucl Med 2007; 48: 1741-1748.
[103] Maddahi J. Properties of an ideal PET perfusion tracer: new PET tracer cases and data. J Nucl Cardiol 2012; 19 Suppl 1: S30-37.
[104] Yu M, Nekolla SG, Schwaiger M and Robinson SP. The next generation of cardiac positron emission tomography imaging agents: discovery of flurpiridaz F-18 for detection of coronary disease. Semin Nucl Med 2011; 41: 305-313.
[105] Gaemperli O and Kaufmann PA. PET and PET/CT in cardiovascular disease. Ann N Y Acad Sci 2011; 1228: 109-136.
[106] Weinberg IN, Huang SC, Hoffman EJ, Araujo L, Nienaber C, Grover-McKay M, Dahlbom M and Schelbert H. Validation of PET-acquired input functions for cardiac studies. J Nucl Med 1988; 29: 241-247.
[107] Lin KP, Huang SC, Choi Y, Brunken RC, Schelbert HR and Phelps ME. Correction of spillover radioactivities for estimation of the blood time-activity curve from the imaged LV chamber in cardiac dynamic FDG PET studies. Phys Med Biol 1995; 40: 629-642.
[108] Lockwood AH. Absorbed doses of radiation after an intravenous injection of N-13 ammonia in man: concise communication. J Nucl Med 1980; 21: 276-278.
[109] Love WD and Burch GE. A comparison of potassium 42, rubidium 86, and cesium 134 as tracers of potassium in the study of cation metabolism of human erythrocytes in vitro. J Lab Clin Med 1953; 41: 351-362.
[110] Love WD, Romney RB and Burch GE. A comparison of the distribution of potassium and exchangeable rubidium in the organs of the dog, using rubidium. Circ Res 1954; 2: 112-122.
[111] Selwyn AP, Allan RM, L'Abbate A, Horlock P, Camici P, Clark J, O'Brien HA and Grant PM. Relation between regional myocardial uptake of rubidium-82 and perfusion: absolute reduction of cation uptake in ischemia. Am J Cardiol 1982; 50: 112-121.
[112] Yoshinaga K, Klein R and Tamaki N. Generator-produced rubidium-82 positron emission tomography myocardial perfusion imaging-From basic aspects to clinical applications. J Cardiol 2010; 55: 163-173.
[113] Chow BJ, Ananthasubramaniam K, dekemp RA, Dalipaj MM, Beanlands RS and Ruddy TD. Comparison of treadmill exercise versus dipyridamole stress with myocardial perfusion imaging using rubidium-82 positron emission tomography. J Am Coll Cardiol 2005; 45: 1227-1234.
[114] Demer LL, Gould KL, Goldstein RA, Kirkeeide RL, Mullani NA, Smalling RW, Nishikawa A and Merhige ME. Assessment of coronary artery disease severity by positron emission tomography. Comparison with quantitative arteriography in 193 patients. Circulation 1989; 79: 825-835.
[115] Go RT, Marwick TH, MacIntyre WJ, Saha GB, Neumann DR, Underwood DA and Simpfendorfer CC. A prospective comparison of rubidium-82 PET and thallium-201 SPECT myocardial perfusion imaging utilizing a single dipyridamole stress in the diagnosis of coronary artery disease. J Nucl Med 1990; 31: 1899-1905.
[116] Goldstein RA, Mullani NA, Marani SK, Fisher DJ, Gould KL and O'Brien HA. Myocardial perfusion with rubidium-82. II. Effects of metabolic and pharmacologic interventions. J Nucl Med 1983; 24: 907-915.
[117] Donato L, Bartolomei G, Federighi G and Torreggiani G. Measurement of coronary blood flow by external counting with radioactive rubidium. Critical appraisal and validation of the method. Circulation 1966; 33: 708-718.
[118] Goldstein RA. Rubidium-82 kinetics after coronary occlusion: temporal relation of net myocardial accumulation and viability in open-chested dogs. J Nucl Med 1986; 27: 1456-1461.
[119] Glover DK and Gropler RJ. Journey to find the ideal PET flow tracer for clinical use: are we there yet? J Nucl Cardiol 2007; 14: 765-768.
[120] Bergmann SR, Fox KA, Rand AL, McElvany KD, Welch MJ, Markham J and Sobel BE. Quantification of regional myocardial blood flow in vivo with H2150. Circulation 1984; 70: 724-733.
[121] Bergmann SR, Herrero P, Markham J, Weinheimer CJ and Walsh MN. Noninvasive quantitation of myocardial blood flow in human subjects with oxygen-15-labeled water and positron emission tomography. J Am Coll Cardiol 1989; 14: 639-652.
[122] Bol A, Melin JA, Vanoverschelde JL, Baudhuin T, Vogelaers D, De Pauw M, Michel C, Luxen A, Labar D and Cogneau M. Direct comparison of [13N]ammonia and [150] water estimates of perfusion with quantification of regional myo-

cardial blood flow by microspheres. Circulation 1993; 87: 512-525.
[123] Herrero P, Kim J, Sharp TL, Engelbach JA, Lewis JS, Gropler RJ and Welch MJ. Assessment of myocardial blood flow using 15O-water and 1-11C-acetate in rats with small-animal PET. J Nucl Med 2006; 47: 477-485.
[124] Iida H, Kanno I, Takahashi A, Miura S, Murakami M, Takahashi K, Ono Y, Shishido F, Inugami A and Tomura N. Measurement of absolute myocardial blood flow with H215O and dynamic positron-emission tomography. Strategy for quantification in relation to the partial-volume effect. Circulation 1988; 78: 104-115.
[125] Miller TR, Wallis JW, Landy BR, Gropler RJ and Sabharwal CL. Measurement of global and regional left ventricular function by cardiac PET. J Nucl Med 1994; 35: 999-1005.
[126] Araujo LI, Lammertsma AA, Rhodes CG, McFalls EO, Iida H, Rechavia E, Galassi A, De Silva R, Jones T and Maseri A. Noninvasive quantification of regional myocardial blood flow in coronary artery disease with oxygen-15-labeled carbon dioxide inhalation and positron emission tomography. Circulation 1991; 83: 875-885.
[127] Hsu B. PET tracers and techniques for measuring myocardial blood flow in patients with coronary artery disease. J Biomed Res 2013; 27: 452-459.
[128] Knuuti J, Kajander S, Mäki M and Ukkonen H. Quantification of myocardial blood flow will reform the detection of CAD. J Nucl Cardiol 2009; 16: 497-506.
[129] Kaufmann PA, Gnecchi-Ruscone T, Yap JT, Rimoldi O and Camici PG. Assessment of the reproducibility of baseline and hyperemic myocardial blood flow measurements with 15O-labeled water and PET. J Nucl Med 1999; 40: 1848-1856.
[130] Maddahi J and Packard RR. Cardiac PET perfusion tracers: current status and future directions. Semin Nucl Med 2014; 44: 333-343.
[131] Schelbert HR, Phelps ME, Huang SC, MacDonald NS, Hansen H, Selin C and Kuhl DE. N-13 ammonia as an indicator of myocardial blood flow. Circulation 1981; 63: 1259-1272.
[132] Walsh WF, Fill HR and Harper PV. Nitrogen-13-labeled ammonia for myocardial imaging. Semin Nucl Med 1977; 7: 59-66.
[133] Bergmann SR, Hack S, Tewson T, Welch MJ and Sobel BE. The dependence of accumulation of 13NH3 by myocardium on metabolic factors and its implications for quantitative assessment of perfusion. Circulation 1980; 61: 34-43.
[134] Shah A, Schelbert HR, Schwaiger M, Henze E, Hansen H, Selin C and Huang SC. Measurement of regional myocardial blood flow with N-13 ammonia and positron-emission tomography in intact dogs. J Am Coll Cardiol 1985; 5: 92-100.
[135] Tamaki N, Yonekura Y, Senda M, Kureshi SA, Saji H, Kodama S, Konishi Y, Ban T, Kambara H and Kawai C. Myocardial positron computed tomography with 13N-ammonia at rest and during exercise. Eur J Nucl Med 1985; 11: 246-251.
[136] Di Carli MF, Dorbala S, Meserve J, El Fakhri G, Sitek A and Moore SC. Clinical myocardial perfusion PET/CT. J Nucl Med 2007; 48: 783-793.
[137] Muzik O, Beanlands RS, Hutchins GD, Mangner TJ, Nguyen N and Schwaiger M. Validation of nitrogen-13-ammonia tracer kinetic model for quantification of myocardial blood flow using PET. J Nucl Med 1993; 34: 83-91.
[138] Yu M, Guaraldi MT, Mistry M, Kagan M, McDonald JL, Drew K, Radeke H, Azure M, Purohit A, Casebier DS and Robinson SP. BMS-747158-02: a novel PET myocardial perfusion imaging agent. J Nucl Cardiol 2007; 14: 789-798.
[139] Maddahi J, Czernin J, Lazewatsky J, Huang SC, Dahlbom M, Schelbert H, Sparks R, Ehlgen A, Crane P, Zhu Q, Devine M and Phelps M. Phase I, first-in-human study of BMS747158, a novel 18F-labeled tracer for myocardial perfusion PET: dosimetry, biodistribution, safety, and imaging characteristics after a single injection at rest. J Nucl Med 2011; 52: 1490-1498.
[140] Yalamanchili P, Wexler E, Hayes M, Yu M, Bozek J, Kagan M, Radeke HS, Azure M, Purohit A, Casebier DS and Robinson SP. Mechanism of uptake and retention of F-18 BMS-747158-02 in cardiomyocytes: a novel PET myocardial imaging agent. J Nucl Cardiol 2007; 14: 782-788.
[141] Huisman MC, Higuchi T, Reder S, Nekolla SG, Poethko T, Wester HJ, Ziegler SI, Casebier DS, Robinson SP and Schwaiger M. Initial characterization of an 18F-labeled myocardial perfusion tracer. J Nucl Med 2008; 49: 630-636.
[142] Nekolla SG, Reder S, Saraste A, Higuchi T, Dzewas G, Preissel A, Huisman M, Poethko T, Schuster T, Yu M, Robinson S, Casebier D, Henke J, Wester HJ and Schwaiger M. Evaluation of the novel myocardial perfusion positron-emission tomography tracer 18F-BMS-747158-02: comparison to 13N-ammonia and validation with microspheres in a pig model. Circulation 2009; 119: 2333-2342.
[143] Berman DS, Maddahi J, Tamarappoo BK, Czernin J, Taillefer R, Udelson JE, Gibson CM, Devine M, Lazewatsky J, Bhat G and Washburn D. Phase II safety and clinical comparison with single-photon emission computed tomography myocardial perfusion imaging for detection of coronary artery disease: flurpiridaz F 18 positron emission tomography. J Am Coll Cardiol 2013; 61: 469-477.

[144] Alpert N, Dean Fang YH and El Fakhri G. Single-scan rest/stress imaging (18)F-labeled flow tracers. Med Phys 2012; 39: 6609-6620.
[145] Higuchi T, Nekolla SG, Huisman MM, Reder S, Poethko T, Yu M, Wester HJ, Casebier DS, Robinson SP, Botnar RM and Schwaiger M. A new 18F-labeled myocardial PET tracer: myocardial uptake after permanent and transient coronary occlusion in rats. J Nucl Med 2008; 49: 1715-1722.
[146] Guehl NJ, Normandin MD, Wooten DW, Rozen G, Sitek A, Ruskin J, Shoup TM, Ptaszek LM, El Fakhri G and Alpert NM. Single-scan rest/stress imaging: validation in a porcine model with 18F-flurpiridaz. Eur J Nucl Med Mol Imaging 2017; 44: 1538-1546.
[147] Mou T, Zhao Z, Fang W, Peng C, Guo F, Liu B, Ma Y and Zhang X. Synthesis and preliminary evaluation of 18F-labeled pyridaben analogues for myocardial perfusion imaging with PET. J Nucl Med 2012; 53: 472-479.
[148] Mou T, Zhao Z, Zhang P, Fang W, Peng C, Lu J, Wang Q, Ma Y and Zhang X. Synthesis and bioevaluation of new (18) F-Labeled pyridaben analogs with improved stability for myocardial perfusion imaging in mice. Chem Biol Drug Des 2015; 86: 351-361.
[149] Sagar S, Liu PP and Cooper LT. Myocarditis. Lancet Lond Engl 2012; 379: 738-747.
[150] Shauer A, Gotsman I, Keren A, Zwas DR, Hellman Y, Durst R and Admon D. Acute viral myocarditis: current concepts in diagnosis and treatment. Isr Med Assoc J 2013; 15: 180-185.
[151] Beyer T, Townsend DW, Brun T, Kinahan PE, Charron M, Roddy R, Jerin J, Young J, Byars L and Nutt R. A combined PET/CT scanner for clinical oncology. J Nucl Med 2000; 41: 1369-1379.
[152] Ozawa K, Funabashi N, Daimon M, Takaoka H, Takano H, Uehara M and Kobayashi Y. Determination of optimum periods between onset of suspected acute myocarditis and ^{18}F-fluorodeoxyglucose positron emission tomography in the diagnosis of inflammatory left ventricular myocardium. Int J Cardiol 2013; 169: 196-200.
[153] Felker GM, Thompson RE, Hare JM, Hruban RH, Clemetson DE, Howard DL, Baughman KL and Kasper EK. Underlying causes and long-term survival in patients with initially unexplained cardiomyopathy. N Engl J Med 2000; 342: 1077-1084.
[154] Cooper LT, Baughman KL, Feldman AM, Frustaci A, Jessup M, Kuhl U, Levine GN, Narula J, Starling RC, Towbin J, Virmani R; American Heart Association; American College of Cardiology; European Society of Cardiology; Heart Failure Society of America; Heart Failure Association of the European Society of Cardiology. The role of endomyocardial biopsy in the management of cardiovascular disease: a scientific statement from the American heart association, the American college of cardiology, and the European society of cardiology. Endorsed by the heart failure society of America and the heart failure association of the European society of cardiology. J Am Coll Cardiol 2007; 50: 1914-1931.
[155] von Olshausen G, Hyafil F, Langwieser N, Laugwitz KL, Schwaiger M and Ibrahim T. Detection of acute inflammatory myocarditis in epstein barr virus infection using hybrid 18F-fluoro-deoxyglucose-positron emission tomography/magnetic resonance imaging. Circulation 2014; 130: 925-926.
[156] Choi JY, Jeong JM, Yoo BC, Kim K, Kim Y, Yang BY, Lee YS, Lee DS, Chung JK and Lee MC. Development of 68Ga-labeled mannosylated human serum albumin (MSA) as a lymph node imaging agent for positron emission tomography. Nucl Med Biol 2011; 38: 371-379.
[157] Lee SP, Im HJ, Kang S, Chung SJ, Cho YS, Kang H, Park HS, Hwang DW, Park JB, Paeng JC, Cheon GJ, Lee YS, Jeong JM and Kim YJ. Noninvasive imaging of myocardial inflammation in myocarditis using 68Ga-tagged mannosylated human serum albumin positron emission tomography. Theranostics 2017; 7: 413-424.
[158] Silverman KJ, Hutchins GM and Bulkley BH. Cardiac sarcoid: a clinicopathologic study of 84 unselected patients with systemic sarcoidosis. Circulation 1978; 58: 1204-1211.
[159] Okumura W, Iwasaki T, Toyama T, Iso T, Arai M, Oriuchi N, Endo K, Yokoyama T, Suzuki T and Kurabayashi M. Usefulness of fasting 18F-FDG PET in identification of cardiac sarcoidosis. J Nucl Med 2004; 45: 1989-1998.
[160] Nishiyama Y, Yamamoto Y, Fukunaga K, Takinami H, Iwado Y, Satoh K and Ohkawa M. Comparative evaluation of 18F-FDG PET and 67Ga scintigraphy in patients with sarcoidosis. J Nucl Med 2006; 47: 1571-1576.
[161] Yamagishi H, Shirai N, Takagi M, Yoshiyama M, Akioka K, Takeuchi K and Yoshikawa J. Identification of cardiac sarcoidosis with (13)N-NH(3)/(18)F-FDG PET. J Nucl Med 2003; 44: 1030-1036.
[162] Tahara N, Tahara A, Nitta Y, Kodama N, Mizoguchi M, Kaida H, Baba K, Ishibashi M, Hayabuchi N, Narula J and Imaizumi T. Heterogeneous myocardial FDG uptake and the disease activity in cardiac sarcoidosis. JACC Cardiovasc Imaging 2010; 3: 1219-1228.
[163] Andrikopoulou E and Bhambhvani P. Optimizing myocardial metabolism for fluorine-18 fluorodeoxyglucose positron emission tomography

imaging of cardiac inflammation. J Nucl Cardiol 2017; [Epub ahead of print].
[164] Lu Y, Grant C, Xie K and Sweiss NJ. Suppression of myocardial 18F-FDG uptake through prolonged high-fat, high-protein, and very-low-carbohydrate diet before FDG-PET/CT for evaluation of patients with suspected cardiac sarcoidosis. Clin Nucl Med 2017; 42: 88-94.
[165] Mc Ardle BA, Leung E, Ohira H, Cocker MS, deKemp RA, DaSilva J, Birnie D, Beanlands RS and Nery PB. The role of F(18)-fluorodeoxyglucose positron emission tomography in guiding diagnosis and management in patients with known or suspected cardiac sarcoidosis. J Nucl Cardiol 2013; 20: 297-306.
[166] Pierre-Louis B, Prasad A and Frishman WH. Cardiac manifestations of sarcoidosis and therapeutic options. Cardiol Rev 2009; 17: 153-158.
[167] Soejima K and Yada H. The work-up and management of patients with apparent or subclinical cardiac sarcoidosis: with emphasis on the associated heart rhythm abnormalities. J Cardiovasc Electrophysiol 2009; 20: 578-583.
[168] Al Moudi M, Sun Z and Lenzo N. Diagnostic value of SPECT, PET and PET/CT in the diagnosis of coronary artery disease: a systematic review. Biomed Imaging Interv J 2011; 7: e9.
[169] Sampson UK, Dorbala S, Limaye A, Kwong R and Di Carli MF. Diagnostic accuracy of rubidium-82 myocardial perfusion imaging with hybrid positron emission tomography/computed tomography in the detection of coronary artery disease. J Am Coll Cardiol 2007; 49: 1052-1058.
[170] Ghosh N, Rimoldi OE, Beanlands RS and Camici PG. Assessment of myocardial ischaemia and viability: role of positron emission tomography. Eur Heart J 2010; 31: 2984-2995.
[171] Schindler TH, Schelbert HR, Quercioli A and Dilsizian V. Cardiac PET imaging for the detection and monitoring of coronary artery disease and microvascular health. JACC Cardiovasc Imaging 2010; 3: 623-640.
[172] Gewirtz H. PET measurement of absolute myocardial blood flow and LV function in dilated cardiomyopathy. JACC Cardiovasc Imaging 2011; 4: 557-560.
[173] Fiechter M, Ghadri JR, Gebhard C, Fuchs TA, Pazhenkottil AP, Nkoulou RN, Herzog BA, Wyss CA, Gaemperli O and Kaufmann PA. Diagnostic value of 13N-ammonia myocardial perfusion PET: added value of myocardial flow reserve. J Nucl Med 2012; 53: 1230-1234.
[174] Santana CA, Folks RD, Garcia EV, Verdes L, Sanyal R, Hainer J, Di Carli MF and Esteves FP. Quantitative (82)Rb PET/CT: development and validation of myocardial perfusion database. J Nucl Med 2007; 48: 1122-1128.
[175] Hajjiri MM, Leavitt MB, Zheng H, Spooner AE, Fischman AJ and Gewirtz H. Comparison of positron emission tomography measurement of adenosine-stimulated absolute myocardial blood flow versus relative myocardial tracer content for physiological assessment of coronary artery stenosis severity and location. JACC Cardiovasc Imaging 2009; 2: 751-758.
[176] Herzog BA, Husmann L, Valenta I, Gaemperli O, Siegrist PT, Tay FM, Burkhard N, Wyss CA and Kaufmann PA. Long-term prognostic value of 13N-ammonia myocardial perfusion positron emission tomography added value of coronary flow reserve. J Am Coll Cardiol 2009; 54: 150-156.
[177] Reddy KG, Nair RN, Sheehan HM and Hodgson JM. Evidence that selective endothelial dysfunction may occur in the absence of angiographic or ultrasound atherosclerosis in patients with risk factors for atherosclerosis. J Am Coll Cardiol 1994; 23: 833-843.
[178] Schindler TH, Nitzsche EU, Olschewski M, Brink I, Mix M, Prior J, Facta A, Inubushi M, Just H and Schelbert HR. PET-measured responses of MBF to cold pressor testing correlate with indices of coronary vasomotion on quantitative coronary angiography. J Nucl Med 2004; 45: 419-428.
[179] Rosas EA, Slomka PJ, García-Rojas L, Calleja R, Jácome R, Jiménez-Santos M, Romero E, Meave A and Berman DS. Functional impact of coronary stenosis observed on coronary computed tomography angiography: comparison with ^{13}N-ammonia PET. Arch Med Res 2010; 41: 642-648.
[180] Tio RA, Dabeshlim A, Siebelink HM, de Sutter J, Hillege HL, Zeebregts CJ, Dierckx RA, van Veldhuisen DJ, Zijlstra F, and Slart RH. Comparison between the prognostic value of left ventricular function and myocardial perfusion reserve in patients with ischemic heart disease. J Nucl Med 2009; 50: 214-219.
[181] Dorbala S, Hachamovitch R, Curillova Z, Thomas D, Vangala D, Kwong RY and Di Carli MF. Incremental prognostic value of gated Rb-82 positron emission tomography myocardial perfusion imaging over clinical variables and rest LVEF. JACC Cardiovasc Imaging 2009; 2: 846-854.
[182] Stanley WC, Hall JL, Stone CK and Hacker TA. Acute myocardial ischemia causes a transmural gradient in glucose extraction but not glucose uptake. Am J Physiol 1992; 262: H91-96.
[183] Depre C and Taegtmeyer H. Metabolic aspects of programmed cell survival and cell death in the heart. Cardiovasc Res 2000; 45: 538-548.
[184] Gropler RJ, Geltman EM, Sampathkumaran K, Pérez JE, Schechtman KB, Conversano A, Sobel BE, Bergmann SR and Siegel BA. Comparison of carbon-11-acetate with fluorine-18-fluo-

rodeoxyglucose for delineating viable myocardium by positron emission tomography. J Am Coll Cardiol 1993; 22: 1587-1597.
[185] Ingelsson E, Sullivan LM, Murabito JM, Fox CS, Benjamin EJ, Polak JF, Meigs JB, Keyes MJ, O'Donnell CJ, Wang TJ, D'Agostino RB, Wolf PA and Vasan RS. Prevalence and prognostic impact of subclinical cardiovascular disease in individuals with the metabolic syndrome and diabetes. Diabetes 2007; 56: 1718-1726.
[186] Tzou WS, Douglas PS, Srinivasan SR, Bond MG, Tang R, Chen W, Berenson GS and Stein JH. Increased subclinical atherosclerosis in young adults with metabolic syndrome: the bogalusa heart study. J Am Coll Cardiol 2005; 46: 457-463.
[187] Tawakol A, Migrino RQ, Bashian GG, Bedri S, Vermylen D, Cury RC, Yates D, LaMuraglia GM, Furie K, Houser S, Gewirtz H, Muller JE, Brady TJ and Fischman AJ. In vivo 18F-fluorodeoxyglucose positron emission tomography imaging provides a noninvasive measure of carotid plaque inflammation in patients. J Am Coll Cardiol 2006; 48: 1818-1824.
[188] Jezovnik MK, Zidar N, Lezaic L, Gersak B and Poredos P. Identification of inflamed atherosclerotic lesions in vivo using PET-CT. Inflammation 2014; 37: 426-434.
[189] Pedersen SF, Sandholt BV, Keller SH, Hansen AE, Clemmensen AE, Sillesen H, Højgaard L, Ripa RS and Kjær A. 64Cu-DOTATATE PET/MRI for detection of activated macrophages in carotid atherosclerotic plaques: studies in patients undergoing endarterectomy. Arterioscler Thromb Vasc Biol 2015; 35: 1696-1703.
[190] Cuhlmann S, Gsell W, Van der Heiden K, Habib J, Tremoleda JL, Khalil M, Turkheimer F, Meens MJ, Kwak BR, Bird J, Davenport AP, Clark J, Haskard D, Krams R, Jones H and Evans PC. In vivo mapping of vascular inflammation using the translocator protein tracer 18F-FEDAA1-106. Mol Imaging 2014; 13.
[191] Kataoka Y, Wolski K, Uno K, Puri R, Tuzcu EM, Nissen SE and Nicholls SJ. Spotty calcification as a marker of accelerated progression of coronary atherosclerosis: insights from serial intravascular ultrasound. J Am Coll Cardiol 2012; 59: 1592-1597.
[192] Aikawa E, Nahrendorf M, Figueiredo JL, Swirski FK, Shtatland T, Kohler RH, Jaffer FA, Aikawa M and Weissleder R. Osteogenesis associates with inflammation in early-stage atherosclerosis evaluated by molecular imaging in vivo. Circulation 2007; 116: 2841-2850.
[193] Beheshti M, Saboury B, Mehta NN, Torigian DA, Werner T, Mohler E, Wilensky R, Newberg AB, Basu S, Langsteger W and Alavi A. Detection and global quantification of cardiovascular molecular calcification by fluoro18-fluoride positron emission tomography/computed tomography--a novel concept. Hell J Nucl Med 2011; 14: 114-120.
[194] Dweck MR, Chow MW, Joshi NV, Williams MC, Jones C, Fletcher AM, Richardson H, White A, McKillop G, van Beek EJ, Boon NA, Rudd JH, Newby DE. Coronary arterial 18F-sodium fluoride uptake: a novel marker of plaque biology. J Am Coll Cardiol 2012; 59: 1539-1548.
[195] Carlin S and Humm JL. PET of hypoxia: current and future perspectives. J Nucl Med 2012; 53: 1171-1174.
[196] Björkerud S and Björkerud B. Apoptosis is abundant in human atherosclerotic lesions, especially in inflammatory cells (macrophages and T cells), and may contribute to the accumulation of gruel and plaque instability. Am J Pathol 1996; 149: 367-380.
[197] Korngold EC, Jaffer FA, Weissleder R and Sosnovik DE. Noninvasive imaging of apoptosis in cardiovascular disease. Heart Fail Rev 2008; 13: 163-173.
[198] Elmore S. Apoptosis: a review of programmed cell death. Toxicol Pathol 2007; 35: 495-516.
[199] Koopman G, Reutelingsperger CP, Kuijten GA, Keehnen RM, Pals ST and van Oers MH. Annexin V for flow cytometric detection of phosphatidylserine expression on B cells undergoing apoptosis. Blood 1994; 84: 1415-1420.
[200] Yagle KJ, Eary JF, Tait JF, Grierson JR, Link JM, Lewellen B, Gibson DF and Krohn KA. Evaluation of 18F-annexin V as a PET imaging agent in an animal model of apoptosis. J Nucl Med 2005; 46: 658-666.
[201] Grierson JR, Yagle KJ, Eary JF, Tait JF, Gibson DF, Lewellen B, Link JM and Krohn KA. Production of [F-18]fluoroannexin for imaging apoptosis with PET. Bioconjug Chem 2004; 15: 373-379.
[202] Murakami Y, Takamatsu H, Taki J, Tatsumi M, Noda A, Ichise R, Tait JF and Nishimura S. 18F-labelled annexin V: a PET tracer for apoptosis imaging. Eur J Nucl Med Mol Imaging 2004; 31: 469-474.
[203] Tenenbaum A and Fisman EZ. Impaired glucose metabolism in patients with heart failure: pathophysiology and possible treatment strategies. Am J Cardiovasc Drugs 2004; 4: 269-280.
[204] Deaton C, Mamas MA, Rutter MK, Gibson M, Bowell S, Byrne R, Coezy K, Gow J and Williams S. Glucose and insulin abnormalities in patients with heart failure. Eur J Cardiovasc Nurs 2011; 10: 75-87.
[205] Kim TN, Kim S, Yang SJ, Yoo HJ, Seo JA, Kim SG, Kim NH, Baik SH, Choi DS and Choi KM. Vascular inflammation in patients with impaired glucose tolerance and type 2 diabetes: analysis with 18F-fluorodeoxyglucose positron

emission tomography. Circ Cardiovasc Imaging 2010; 3: 142-148.
[206] Gleissner CA, Galkina E, Nadler JL and Ley K. Mechanisms by which diabetes increases cardiovascular disease. Drug Discov Today Dis Mech 2007; 4: 131-140.
[207] American Diabetes Association. Diagnosis and classification of diabetes mellitus. Diabetes Care 2011; 34 Suppl 1: S62-69.
[208] Tahara N, Kai H, Yamagishi S, Mizoguchi M, Nakaura H, Ishibashi M, Kaida H, Baba K, Hayabuchi N and Imaizumi T. Vascular inflammation evaluated by [18F]-fluorodeoxyglucose positron emission tomography is associated with the metabolic syndrome. J Am Coll Cardiol 2007; 49: 1533-1539.
[209] Mizoguchi M, Tahara N, Tahara A, Nitta Y, Kodama N, Oba T, Mawatari K, Yasukawa H, Kaida H, Ishibashi M, Hayabuchi N, Harada H, Ikeda H, Yamagishi SI and Imaizumi T. Pioglitazone attenuates atherosclerotic plaque inflammation in patients with impaired glucose tolerance or diabetes a prospective, randomized, comparator-controlled study using serial FDG PET/CT imaging study of carotid artery and ascending aorta. JACC Cardiovasc Imaging 2011; 4: 1110-1118.
[210] Nitta Y, Tahara N, Tahara A, Honda A, Kodama N, Mizoguchi M, Kaida H, Ishibashi M, Hayabuchi N, Ikeda H, Yamagishi S and Imaizumi T. Pioglitazone decreases coronary artery inflammation in impaired glucose tolerance and diabetes mellitus: evaluation by FDG-PET/CT imaging. JACC Cardiovasc Imaging 2013; 6: 1172-1182.
[211] Liao HW, Saver JL, Wu YL, Chen TH, Lee M and Ovbiagele B. Pioglitazone and cardiovascular outcomes in patients with insulin resistance, pre-diabetes and type 2 diabetes: a systematic review and meta-analysis. BMJ Open 2017; 7: e013927.
[212] Aronoff S, Rosenblatt S, Braithwaite S, Egan JW, Mathisen AL, and Schneider RL. Pioglitazone hydrochloride monotherapy improves glycemic control in the treatment of patients with type 2 diabetes: a 6-month randomized placebo-controlled dose-response study. The Pioglitazone 001 Study Group. Diabetes Care 2000; 23: 1605-1611.
[213] Giacca A, Xiao C, Oprescu AI, Carpentier AC and Lewis GF. Lipid-induced pancreatic β-cell dysfunction: focus on in vivo studies. Am J Physiol Endocrinol Metab 2011; 300: E255-262.
[214] Knuuti J, Takala TO, Någren K, Sipilä H, Turpeinen AK, Uusitupa MI and Nuutila P. Myocardial fatty acid oxidation in patients with impaired glucose tolerance. Diabetologia 2001; 44: 184-187.
[215] Herrero P, Peterson LR, McGill JB, Matthew S, Lesniak D, Dence C and Gropler RJ. Increased myocardial fatty acid metabolism in patients with type 1 diabetes mellitus. J Am Coll Cardiol 2006; 47: 598-604.
[216] Labbé SM, Grenier-Larouche T, Croteau E, Normand-Lauzière F, Frisch F, Ouellet R, Guérin B, Turcotte EE and Carpentier AC. Organ-specific dietary fatty acid uptake in humans using positron emission tomography coupled to compute tomography. Am J Physiol Endocrinol Metab 2011; 300: E445-453.
[217] Labbé SM, Noll C, Grenier-Larouche T, Kunach M, Bouffard L, Phoenix S, Guérin B, Baillargeon JP, Langlois MF, Turcotte EE, Carpentier AC. Improved cardiac function and dietary fatty acid metabolism after modest weight loss in subjects with impaired glucose tolerance. Am J Physiol Endocrinol Metab 2014; 306: E1388-1396.
[218] Labbé SM, Grenier-Larouche T, Noll C, Phoenix S, Guérin B, Turcotte EE and Carpentier AC. Increased myocardial uptake of dietary fatty acids linked to cardiac dysfunction in glucose-intolerant humans. Diabetes 2012; 61: 2701-2710.
[219] Ménard SL, Croteau E, Sarrhini O, Gélinas R, Brassard P, Ouellet R, Bentourkia M 'hamed, van Lier JE, Des Rosiers C, Lecomte R and Carpentier AC. Abnormal in vivo myocardial energy substrate uptake in diet-induced type 2 diabetic cardiomyopathy in rats. Am J Physiol Endocrinol Metab 2010; 298: E1049-1057.
[220] Prior JO, Quiñones MJ, Hernandez-Pampaloni M, Facta AD, Schindler TH, Sayre JW, Hsueh WA and Schelbert HR. Coronary circulatory dysfunction in insulin resistance, impaired glucose tolerance, and type 2 diabetes mellitus. Circulation 2005; 111: 2291-2298.
[221] Di Carli MF, Charytan D, McMahon GT, Ganz P, Dorbala S and Schelbert HR. Coronary circulatory function in patients with the metabolic syndrome. J Nucl Med 2011; 52: 1369-1377.
[222] Kircher M and Lapa C. Novel noninvasive nuclear medicine imaging techniques for cardiac inflammation. Curr Cardiovasc Imaging Rep 2017; 10: 6.
[223] Knetsch PA, Petrik M, Griessinger CM, Rangger C, Fani M, Kesenheimer C, von Guggenberg E, Pichler BJ, Virgolini I, Decristoforo C and Haubner R. [68Ga]NODAGA-RGD for imaging αvβ3 integrin expression. Eur J Nucl Med Mol Imaging 2011; 38: 1303-1312.
[224] Haubner R, Finkenstedt A, Stegmayr A, Rangger C, Decristoforo C, Zoller H and Virgolini IJ. [(68)Ga]NODAGA-RGD-metabolic stability, biodistribution, and dosimetry data from patients with hepatocellular carcinoma and liver cirrho-

sis. Eur J Nucl Med Mol Imaging 2016; 43: 2005-2013.
[225] Grönman M, Tarkia M, Kiviniemi T, Halonen P, Kuivanen A, Savunen T, Tolvanen T, Teuho J, Käkelä M, Metsälä O, Pietilä M, Saukko P, Ylä-Herttuala S, Knuuti J, Roivainen A and Saraste A. Imaging of $\alpha_v\beta_3$ integrin expression in experimental myocardial ischemia with [68Ga] NODAGA-RGD positron emission tomography. J Transl Med 2017; 15: 144.
[226] Keliher EJ, Ye YX, Wojtkiewicz GR, Aguirre AD, Tricot B, Senders ML, Groenen H, Fay F, Perez-Medina C, Calcagno C, Carlucci G, Reiner T, Sun Y, Courties G, Iwamoto Y, Kim HY, Wang C, Chen JW, Swirski FK, Wey HY, Hooker J, Fayad ZA, Mulder WJ, Weissleder R and Nahrendorf M. Polyglucose nanoparticles with renal elimination and macrophage avidity facilitate PET imaging in ischaemic heart disease. Nat Commun 2017; 8: 14064.
[227] Phenix CP, Rempel BP, Colobong K, Doudet DJ, Adam MJ, Clarke LA and Withers SG. Imaging of enzyme replacement therapy using PET. Proc Natl Acad Sci U S A 2010; 107: 10842-10847.
[228] Ali M, Pulli B and Chen JW. Molecular imaging of macrophage enzyme activity in cardiac inflammation. Curr Cardiovasc Imaging Rep 2014; 7: 9258.
[229] Quillard T, Croce K, Jaffer FA, Weissleder R and Libby P. Molecular imaging of macrophage protease activity in cardiovascular inflammation in vivo. Thromb Haemost 2011; 105: 828-836.
[230] Craig VJ, Zhang L, Hagood JS and Owen CA. Matrix metalloproteinases as therapeutic targets for idiopathic pulmonary fibrosis. Am J Respir Cell Mol Biol 2015; 53: 585-600.
[231] Perišić Nanut M, Sabotič J, Jewett A and Kos J. Cysteine cathepsins as regulators of the cytotoxicity of NK and T cells. Front Immunol 2014; 5: 616.
[232] Cheng XW, Huang Z, Kuzuya M, Okumura K and Murohara T. Cysteine protease cathepsins in atherosclerosis-based vascular disease and its complications. Hypertension 2011; 58: 978-986.
[233] Shi GP, Bryant RA, Riese R, Verhelst S, Driessen C, Li Z, Bromme D, Ploegh HL and Chapman HA. Role for cathepsin F in invariant chain processing and major histocompatibility complex class II peptide loading by macrophages. J Exp Med 2000; 191: 1177-1186.
[234] Riese RJ and Chapman HA. Cathepsins and compartmentalization in antigen presentation. Curr Opin Immunol 2000; 12: 107-113.